Julia Grill

Optimizing Crystallization Conditions in a Continuous Process: Simulations and Experimental Investigations

DIPLOMA THESIS

Zur Erlangung des akademischen Grades einer Diplomingenieurin
der Studienrichtung Verfahrenstechnik

erreicht an der
Technischen Universität Graz
Februar 2012

Advisors:
Univ. Prof. Dipl.-Ing. Dr. techn. J. Khinast
and
Dipl.-Ing. R. Eder

Institute for Process and Particle Engineering
Graz University of Technology

Declaration

The work presented in this diploma thesis is to the best of my knowledge and belief, original, except as acknowledged in the text. This material has not been submitted, either in the whole or in part, for a degree at this or any other university.

_____ _____

Place, Date Signature

Eidesstattliche Erklärung

Ich erkläre an Eides Statt, dass ich die vorliegende Arbeit selbstständig und ohne fremde Hilfe verfasst, andere als die angegebenen Quellen nicht benutzt und die den benutzten Quellen wörtlich und inhaltlich entnommenen Stellen als solche kenntlich gemacht habe. Ich versichere, dass ich dieses Diplomarbeitsthema bisher weder im In- noch im Ausland in irgendeiner Form als Prüfungsarbeit vorgelegt habe.

_____ _____

Ort, Datum Unterschrift

Abstract

The aim of the presented diploma thesis is the investigation the crystallization of acetylsalicylic acid (ASA) from an ethanolic solution in a continuously seeded, continuously operated tubular crystallizer (CSCOTC). In this project, the reactor consists of a 15m long silicon tube with an inner diameter of 2mm. A suspension stream with a defined mass of solid seed particles was mixed with a slightly undersatured solution and was fed into the reactor. In the reactor supersaturation was achieved by cooling, as the supersaturation level strongly depends on the temperature and is the driving force for crystallization. Therefore, the crystal growth can be directly influenced by controlling the cooling rate.

In the first stage, a MatLab® program was developed to optimize a cooling trajectory which allows a rising supersaturation level with increasing retention time. Thus, the crystal growth can be enhanced without the risk of blocking the reactor.

Due to the small diameter of the reactor, the crystallization heat is dissipated instantaneously, thus the temperature and concentration gradient in radial direction can be neglected.

Subsequently, the reactor was adapted to the optimized temperature profile and then the influence of the retention time on the crystal growth process was investigated. The results agree with theoretical expectations and express the direct proportion between retention time and crystal growth.

To evidence that crystal growth is not based on agglomeration and crystal intergrowth, the mass gain of product also increased constantly with increasing retention time.

In order to verify the obtained results, the reactor was applied in the production of acetaminophen (paracetamol), another active pharmaceutical ingredient, based on the adapted simulation in MatLab®.

Similar to the results obtained for ASA, all experiments with paracetamol were operated successfully and resulted both in an increasing crystal growth and mass gain. Based on the smaller temperature dependence of the solubility of paracetamol, the seed particle size is a determining factor of the crystal growth. Due to the higher volume-to-mass ratio of smaller seed particles, minor growth rates have been achieved.

To conclude the work, he experimental results and simulations were compared to verify the limiting assumptions (e.g., the absence of nucleation, agglomeration and breakage or no particle size distribution).

Kurzfassung

In der vorliegenden Arbeit wurde die kontinuierliche Kristallisation von Acetylsalicylsäure (ASA) aus Ethanol in einem Rohrreaktor untersucht. Der Reaktor besteht aus einem 15m langen Silikonschlauch mit einem Innendurchmesser von 2mm. Eine mit Impfkristallen beladene Suspensionslösung wird mit einer leicht untersättigten Lösung gemischt und dem Reaktor zugeführt in welchem mittels Kühlung ein Zustand ständiger Übersättigung erreicht wird, die letztlich zum Kristallwachstum führt. Der Grad der Übersättigung ist verantwortlich für das Wachstumspotential der Impfkristalle und kann, da er im Falle der Testsubstanz stark temperaturabhängig ist, über die Kontrolle der Reaktorkühlung beeinflusst werden.

In diesem Sinne wurde mit Hilfe der Simulation in MatLab® eine Kühlstrecke entwickelt, deren Kühlprofil einen mit zunehmender Retentionszeit steigenden Übersättigungsgrad erlaubt und somit größeres Kristallwachstum ermöglicht, ohne den Reaktor der Gefahr des Verstopfens auszusetzen.

Dank des geringen Reaktordurchmessers kann die Kristallisationswärme rasch abgeführt und eine Temperatur- und Konzentrationsverteilung in radialer Richtung vernachlässigt werden.

Nach Optimierung des Kühlprofils wurde der Einfluss der Retentionszeit auf das Kristallwachstum untersucht und zeigte, wie erwartet, größeres Wachstum der Kristalle bei steigenden Retentionszeiten.

Weiters wurde der bestehende Versuchsaufbau für die Kristallisation einer weiteren Testsubstanz, in diesem Fall Paracetamol, adaptiert. Grundlegend dafür war ebenfalls die Simulation in MatLab®, welche an das abweichende Löslichkeitsverhalten angepasst werden musste.

Alle Versuche mit Paracetamol verliefen erfolgreich und zeigten sowohl ein Kristallwachstum der Impfkristalle als auch eine Zunahme im Massenfluss des auskristallisierten Produktes. Da die Löslichkeit von Paracetamol geringer temperaturabhängig als jene von ASA ist, spielt die Größe der Impfkristalle auf das Kristallwachstum eine entscheidende Rolle. Aufgrund des höheren Volumen-zu-Masse-Verhältnisses von kleinen Impfkristallen werden niedrigere Wachstumsraten erzielt.

Abschließend wurden die Ergebnisse aus den Laborversuchen mit jenen aus der Simulation verglichen, um die getroffenen Einschränkungen (keine Nukleation, keine Agglomeration, kein Partikelabrieb sowie keine Korngrößenverteilung) zu untersuchen.

Table of Contents

List of Figures

List of Tables

Abbreviations

Name	Unit	Description
ASA		acetylsalicylic acid
API		active pharmaceutical ingredient
CSCOTC		continuously seeded, continuously operated tubular crystallizer
EtOH		Ethanol
IBU		ibuprofen
PAC		paracetamol, acetaminophen
PI		peristaltic pump
PII		peristaltic pump
PSD		Particle Size Distribution
$q_0(x)$		number based particle size distribution
$q_3(x)$	1/mm	volume based particle size distribution
VMD	µm	volume mean diameter
WB		waterbath

Nomenclature

Name	Unit	Description
c	mol/l	concentration
c^*	mol/l	equilibrium concentration
c_p	J/kgK	heat capacity
d_{inner}	mm	inner diameter
d_{outer}	mm	outer diameter
d_p	µm	particle diameter
$d_{p,seed}$	µm	seed particle size
F_{shape}	-	shape factor
K_g	m/s	mass transfer coefficient of model substance
$k_{heat,tot}$	W/m^{2}K	overall heat transfer coefficient
L	M	Length of the tubing
$m_{dissolved\ ASA}/m_{EtOH}$	kg$_i$/kg	mass fraction of ASA in pure EtOH
$m_{dissolved\ PAC}/m_{EtOH}$	kg$_i$/kg	mass fraction of PAC in pure EtOH
$\dot{m}_{EtOH}$	kg/s	mass flow rate of feed solution
$m_{EtOH,EtOH}$	kg	mass of EtOH in the feed solution
$\dot{m}_{EtOH,feed}$	kg/s	mass flow of pure EtOH in the entering stream
$\dot{m}_{feed}$	kg/s	total feed mass flow rate
$\dot{m}_{seed}$	kg/s	mass flow rate of seed suspension
$m_{subst,EtOH}$	kg	mass of substance in the feed solution
MW	kg/kmol	molar weight
N	-	number of particles
N_{conc}	1/m^3	particle concentration in the entering stream
N_1, N_2, N_3	-	Nyvlt parameters
Nu	-	Nusselt number
$\dot{Q}$	W	heat transfer rate
$\dot{Q}_{EtOH}$	m^3/s	volume flow rates of feed solution
$\dot{Q}_{seed}$	m^3/s	volume flow rate of seed suspension
S	-	Supersaturation

Name	Unit	Description
T	K	temperature
T_{amb}	°C	ambient temperature of the waterbath
T_{bath}	°C	temperature of the cooling bath
$T_{reactor}$	°C	crystallization temperature
$T(x)$	°C	temperature profile along the tubing
w	kg_i/kg	mass fraction
$w_{diss,feed}$	kg_i/kg	mass fraction of dissolved substance
$w_{diss,seed}$	kg_i/kg	equilibrium mass fraction
$w_{diss}(x)$	kg_i/kg	dissolved substance along the tubing
w_{EtOH}	kg_i/kg	mass fraction of dissolved substance in the feed solution
w_{seed}	kg_i/kg	total mass fraction in the seed suspension
w_{solid}	kg_i/kg	solid mass fraction
$w_{solid,feed}$	kg_i/kg	mass fraction of solid substance in the mixing zone
x^*	mol_i/mol_{EtOH}	molar fraction of substance I in pure EtOH
α_{inner}	W/mm^2K	inner heat transfer coefficient
α_{outer}	W/mm^2K	outer heat transfer coefficient
Δh_{crist}	J/kg	heat of crystallization
Δh_f	J/mol	fusion enthalpy
λ	W/mK	heat conductivity
λ_{tubing}	W/mK	transfer conductivity of the tubing
$\mu_{i,solid}$	J/mol	chemical potential of the solid phase
$\mu_{i,solution}$	J/mol	chemical potential of the solution
ρ	kg/m^3	density
ρ_{EtOH}	kg/m^3	density of EtOH
ρ_{feed}	kg/m^3	density of the entering stream
ρ_{subst}	kg/m^3	density of model substance
$\rho_{subst,sat}(T)$	kg/m^3	partial saturation density of the model substance at temperature T

1. INTRODUCTION

1.1. CRYSTALS AND CRYSTALLIZATION

In contrast to amorphous structures, crystals are solids whose atoms, ions or molecules are arranged in three-dimensional, .in a periodic repetition, so-called lattice.
Depending on the spatial periodic arrangement of the components we distinguish seven different crystal systems (monoclinic, triclinic, prismatic, tetragonal, hexagonal, trigonal-rhombohedral and cubic).
Crystals display a range of habits, such as plates, prismatic or needle shaped particles. Needle shaped or platy particles are undesired in commercial relevant processes (classification, flowability, cracking, packing, filtering), as they cause difficulties in handling the product.
Crystallization is the phase transfer of a substance from the liquid (solution or melt) into the solid state. Technologically it is used to separate and purify compounds. Components in solid form offer a wide range of advantages, e.g. low reactivity, high purity as well as easy operation (storage, transport, packaging, mixing, dosing, etc.).
Crystals often emerge in various packing arrangements of the same molecules [9] and therefore in different lattice structures.[22] This phenomenon is called polymorphism and leads to different physicochemical properties [24], e.g. solubility and dissolution rate, density, melting point or structural stability. Pseudo-polymorphism refers to crystals with incorporated solvate molecules into the crystal structure (so called solvates or hydrates, if water is the solvate). The type of polymorph formed depends on the external conditions during the crystallization step.

In the pharmaceutical industry over 90% of all active pharmaceutical ingredients (APIs) are crystals of small organic molecules, which indicates the relevance of crystallization as an important aspect.[3]

The process of transferring a dissolved substance from the liquid or gaseous phase into a solid state and can be distinguished by the generation of supersaturation, e.g.

- By cooling
- By evaporation of solvent, e.g. by vacuum
- By changing the solution composition
- By chemical reactions

Crystallization by cooling is preferred for substances with a strong dependence of solubility on the temperature and is the basis of the presented work.

1.1.1. SUPERSATURATION

Supersaturation is the driving force for crystallization. Supersaturation ratio *S* is defined as the ratio between the equilibrium concentration *c** at a given temperature and a present concentration *c* as shown in Eq. 1.[18, 25]

$$S = \frac{c}{c^*} \qquad \textbf{Eq. 1}$$

At supersaturation conditions the chemical potential of the solid phase $\mu_{i,solid}$ is less than the chemical potential of the solution $\mu_{i,solution}$:

$$\mu_{i,solid} < \mu_{i,solution} \qquad \textbf{Eq. 2}$$

As a consequence, the system tries to balance this equation by nucleation and/or crystal growth.

In **Figure 1-1** a common saturation – supersaturation gradient is depicted. Primarily the saturation line subdivides the graph into an undersaturated and a supersaturated zone. A stable zone can only exist in undersaturated solutions. In supersaturated solutions the metastable limit defines the labile and the metastable zone.

In the stable zone equilibrium concentration is not achieved and nucleation cannot occur. At higher temperatures or concentrations, respectively, the system passes over into the metastable zone.. Under these conditions crystal growth is possible, but only in the labile zone spontaneous nucleation can be enforced.

The crystallization process which is dealt with in this work is indicated by the arrow in the figure. The process starts under slightly undersaturated conditions and reaches the metastable zone via cooling, where crystal growth occurs. For precipitation processes of nuclei the supersaturation needs to be increased until the labile zone is reached.

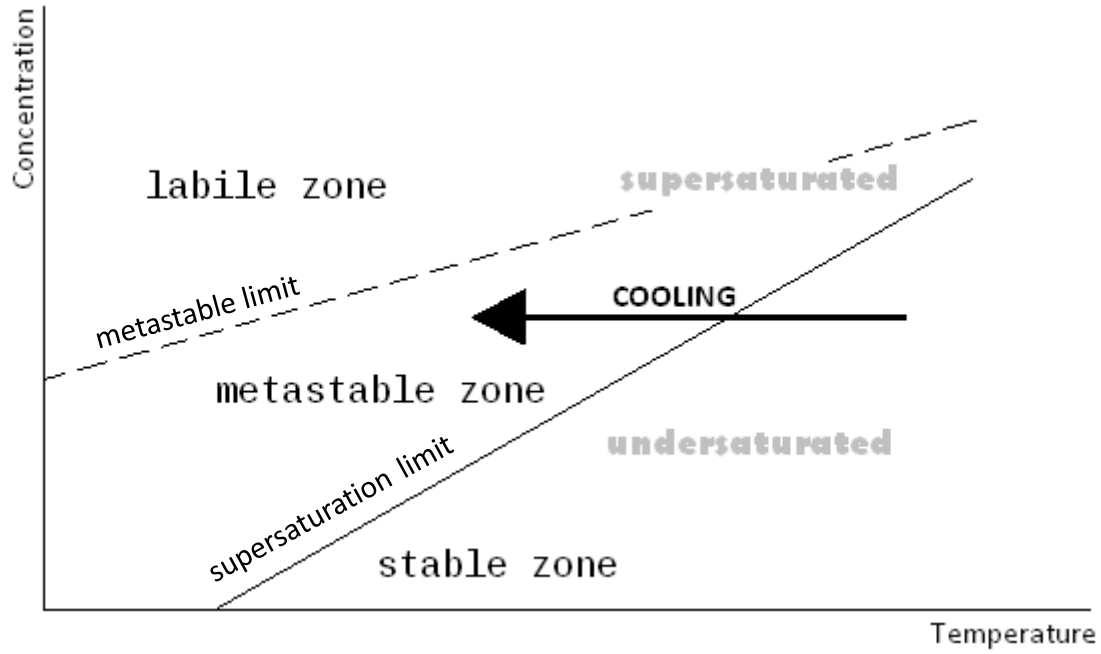

Figure 1-1: undersaturated and supersaturated solution according to the temperature

adapted from Mullin, Butterworth-Heinemann, 1992

1.1.2. TEMPERATURE PROFILES

The most facile way of cooling is a natural cooling trajectory which can be provided via air cooling, for example. The solid line shown in **Figure 1-2** expresses this single-stage cooling process. The cooling rate in the beginning of the crystallization is high and decreases during the process. Because of the high supersaturation level at the beginning of the crystallization this should not be the preferred cooling for the investigated process, nevertheless good experimental results have been achieved [2].

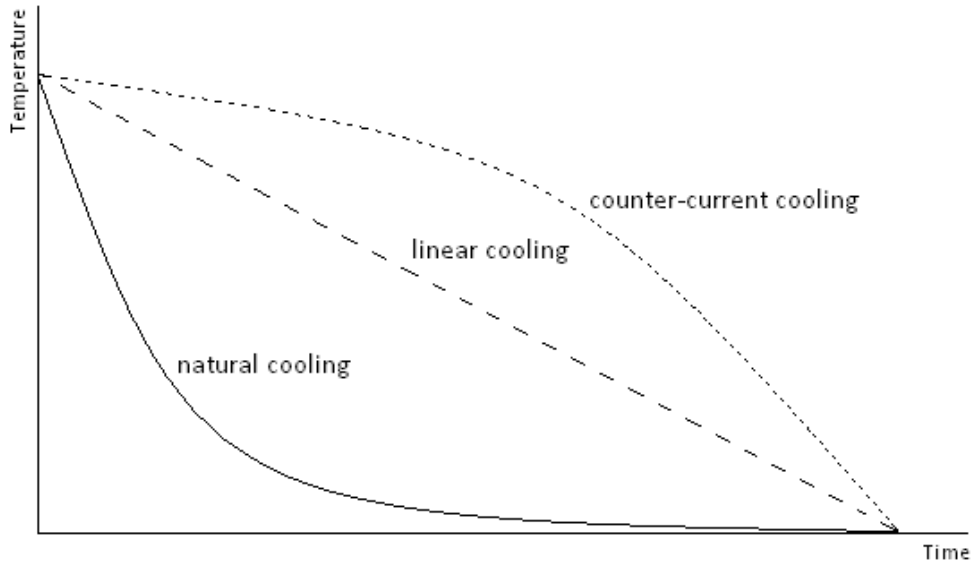

Figure 1-2: schematic temperature profiles for different cooling rates

The more controlled cooling would be a linear cooling, shown as a dashed line in **Figure 1-2**, enabled by constant cooling steps. The supersaturation would get lower at the end of the process, which prevented complete crystallization.

The optimum cooling trajectory according to a constant supersaturation is a counter-current cooling. In a supersaturated solution, the crystal growth consumes the supersaturation. In order to crystallize at constant supersaturation conditions, it is necessary to adjust the cooling to the increasing crystal surface. Towards the end of a crystallization batch, the seeds have already grown and offer, therefore, larger surface areas. Thus the cooling trajectory becomes steeper. Hence supersaturation can be consumed at a faster rate at this state of the crystallization process.

To approximate this cooling profile, a large number of waterbaths is needed.

1.1.3. NUCLEATION AND CRYSTAL GROWTH

Nucleation is the birth of new crystal nuclei from solution.
In the literature three mechanisms of nucleation are described [13]:

- Primary homogenous nucleation (no particles in solution available)
- Primary heterogeneous nucleation (in presence of foreign particles)
- And secondary nucleation (in presence of species-specific particles).

Primary homogenous nucleation only occurs for highly concentrated solutions as demonstrated in **Figure 1-3**. The solid line expresses the equilibrium solubility and therefore the stable limit for crystallization, whereas the dashed lines mark the metastable limits for primary homogenous, primary heterogenous and secondary nucleation. In industrial crystallization the presence of abraded particles or seeds can usually not be avoided and hence secondary nucleation is the most frequently mechanism.

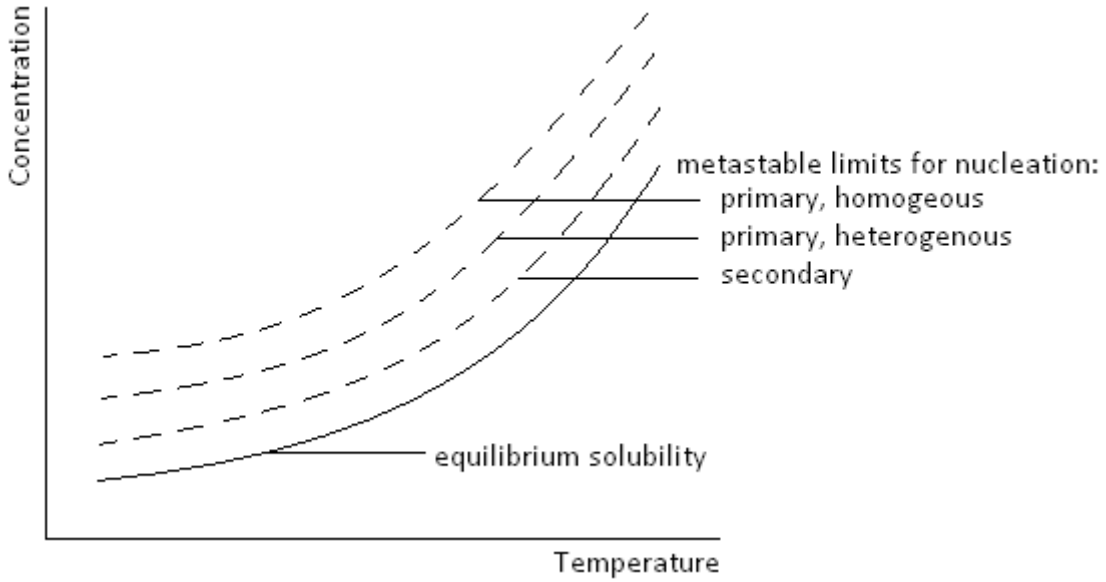

Figure 1-3: metastable supersaturation for different types of nucleation

adapted from Hofmann Guenter, 2004

Crystal growth is the increase in mass of crystals through incorporation of molecules from the feed solution. This, elementary particles are first transported to the crystal via diffusion or convection and then integrated into the crystal surface.

1.2. CONTINUOUS SEEDED, CONTINUOUS OPERATED TUBULAR CRYSTALLIZER (CSCOTC)

Today, most crystallization processes in the pharmaceutical industry are performed traditionally batch-wise.[6] The advantages of batch-wise API production range from an easy implementation and maintenance of the equipment or the easy adaptability of one device for several substances, to the suitability for viscous and toxic substances to no limitation of crystal growth. [10]

In contrast, continuous processes offer a wide range of benefits. The main advantage is the elimination of batch to batch variability of product properties and the better trimming to optimal conditions. [20] In general, shorter down times can be established. Especially for the adoption of a test scaled system into a high performance industry scale, continuous processes involve less scale-up difficulties via numbering-up. Due to shorter down times, smaller equipment like crystallizers, energy supply units or heat exchangers can be used. However several feed- and product tanks could become necessary, if the supply of raw material and the demand of product cannot be held constant.

Nevertheless, these enormous advantages of continuous manufacturing are widely used in the chemical industry, and pharmaceutical companies now get more and more interested in this technology.

The continuous seeded, continuous operated tubular crystallizer (CSCOTC) operates basically like a continuous block flow reactor. For the presented investigations, the reactor consists of a 15 m long, coiled silicone hose with an inner diameter of 2 mm.

In a continuous block flow reactor infinitesimally thin volume slices move through the reactor without mixing or exchange of material and/or heat. The concentration of the reagents is always a function of the axial position in the tube. This assumption is best achieved with thin, long tubes. In this case no concentration/temperature profile occurs in radial direction and it is legitimate to develop a profile along the axis. Further assumptions can be made such as no back-mixing or no storage takes place.

1.2.1. HEAT TRANSFER

The control of the process temperature necessitates knowledge about the heat transfer rate through the reactor wall to define the temperature of the cooling baths.
The heat transfer rate $\dot{Q}$ [W] is defined as:

$$\dot{Q} = k_{heat,tot} * d_{outer} * \pi * L * (T_{reactor} - T_{bath}) \quad \textbf{Eq. 3}$$

where $k_{heat,tot}$ denotes the overall heat transfer coefficient [W/m^{2}K], d_{outer} the outer diameter [mm] and L the length [m] of the tubing, $T_{reactor}$ the crystallization temperature inside the reactor and T_{bath} the temperature of the cooling bath.

$k_{heat,tot}$ is expressed by:

$$k_{heat,tot} = \frac{\frac{1}{d_{outer}}}{\frac{1}{d_{inner} * \alpha_{inner}} + \frac{ln\frac{d_{outer}}{d_{inner}}}{\lambda_{tubing}} + \frac{1}{d_{outer} * \alpha_{outer}}} \quad \textbf{Eq. 4}$$

Here d_{inner} is the inner diameter of the tubing; λ_{tubing} [W/mK] is the heat transfer conductivity of the tubing and therefore a fixed material constant. α_{inner} and α_{outer} [W/mm^{2}K] refer to the heat transfer coefficient at the inside and outside of the tubing and depend on the fluid and the flow conditions.

1.3. PARTICLE SIZE DISTRIBUTION (PSD)

Industrial practice usually does not work with one well-defined particle size, but with a mix of different particle sizes. This mix is described by the particle size distribution (PSD). The size of particles in pharmaceutical processes reaches from nanometers up to millimeters. Hence, lots of physical particle properties are influenced by the particles size and/or the PSD.

In the following, some examples are mentioned. For a single particle the strength or agglomeration tendency increases with decreasing particle size. For a collective the separability decreases, while on the other hand, the specific surface or solubility increases with decreasing particle sizes. Collectives with a broad PSD have a stronger tendency to segregate (smaller particles of the collective move easily into spaces between the large particles and so large particles migrate upwards).

There are several expressions to describe the PSD, which are mathematically interconvertable. In practice the volume based particle size distribution $q_3(x)$ is mainly used. This description of a collective sorts particles according to their volume (or, for a constant density as well their mass) and refers to the particle diameters. The information about the $q_3(x)$-distribution is mainly required to create mass balances or material flows in industrial processes. The $q_3(x)$-distribution can be determined by sieving or sedimentation.

Another description of collectives is the $q_0(x)$-distribution, which sorts the number of particles with a defined diameter into classes. This concept can be used to prove the quality of a collective (that no fines have been produced, e.g.). Analysis usually performed with Coulter-Counter or image analysis like microscope or QICPIC.

Furthermore, for non-spherical particles there is a wide number of concepts to describe irregularly shaped particles, for example different types of measured diameters (Feret-diameter, projected diameter,…) or comparison to a spheric particle with identical properties (surface, volume, settling velocity,…).

1.3.1. PSD ANALYSIS BY QICPIC

The PSD analysis by QICPIC is an image analysis, launched by Symantec. It allows particle size and shape analysis from 1 µm to 20 mm as well as calculations of size and shape characteristics. Low statistical errors due to very high numbers of analyzed particles can be guaranteed. Agglomeration and superposition of particles, as well as multiple counting can be avoided.

1.4. STATE OF THE ART

The continuous production of organic particles is an increasingly significant process in the industrial production of pharmaceutical substances. This is reflected by a number of patents and publications in the field. In the following, a brief overview of the current state of the art is given.

In the patent of Midler, impinging fluid jet streams, containing high supersaturated mother liquor, are used to achieve high intensive micromixing of fluids prior to start nucleation. [26] Also Brenek described a method for crystallization using API-contained fluid jet streams, impinging on a plate where micromixing, reaction and nucleation occur. [15] Both methods base on very high supersaturations. This leads do significant problems, i.e. that nucleation of organic compounds frequently hampered under high supersaturation conditions and amorphous material could be produced instead of crystals. Also the absence of polymorphs cannot be guaranteed. [17]

Myerson presented in his patent on molecular crystals a continuous micro-reactor for producing nanometer- and micron-sized particles for direct inhalation in a range of 1 – 3 micron. To avoid the problems caused by high supersaturation, he worked at modest supersaturation levels and controls the crystal growth by restricting the size of the crystallization domain. [17]

Dombrowski explained a crystallization method of alpha-lactose in a two-step apparatus: in the first stage monodisperse drops of mother liquor were produced, which are continuously cooled in a tubular crystallizer to fall below the saturation limit. Hence the crystals grow in each single drop. [7]

For the continuous nanoparticle production of 2,2'-dipyridylamine by microfluidic-based emulsion, mixing and crystallization, Su used a three T-junction micro-mixer. [8]

A related microfluidic device has been used by Gerts for a time-controlled separation by seeding of nucleation and growth stages of proteins. [12]

The patent of Schiewe and Zierenberg described a method for crystallizing inhalable medicaments in a tubular crystallizer. To avoid blocking, a segmented flow was used. To this, a stream of dissolved substance and a transport medium enter alternating the reactor. [16]

Alvarez and Myerson crystallized organic compounds in a nonconventional block flow reactor by increasing the concentration of antisolvent. Static mixers in the reactor were used to promote homogenous mixing. The influence of supersaturation on the crystal growth was investigated.[3]

Gros described in his publication a model about simulating the behavior of slow growing crystals in a continuous vertical crystallizer, based on the assumptions of steady state conditions, size-dependent growth, no growth rate dispersion or settling of crystals and neither nucleation nor breakage. [20]

In the work of Mendez des Rio a tubular apparatus was used to rapidly cool supersaturated ethanolic or methanolic solutions of paracetamol to fall below the solubility limit. After nucleation the crystals grew both in a tubular device as well as in a stirred vessel. [11]

The advantages of continuous processing in terms of process (especially shorter down times), operation and costs compared to a batch process were investigated by Lawton using a continuous oscillatory baffled crystallizer. [4]

In summary, the broad number of publications established above shows the importance of continuous processes in the current research.

Inspired by the versatility of the CSCOTC reactor and the diversity of strategies, a novel, versatile, continuously seeded, continuously operated tubular crystallizer system (CSCOTC) for the crystallization of active pharmaceutical ingredients (APIs) under controlled conditions was developed and tested at the Institute of Process and Particle Engineering in the working group of Dipl.-Ing. Dr. Heidi Gruber-Wölfler.[2] In this apparatus, single process parameters can be controlled independently. The aim of the presented work is to optimize the given

process conditions and to achieve a better process control. In order to test the versatility of the system, it was furthermore applied to another model substance.

1.5. MOTIVATION AND GOALS

As part of an earlier study of the IPPT (Institute for Particle and Process Engineering, TU Graz) a continuous block flow reactor for crystallization was developed and successfully operated. To optimize the setup the single-stage air cooling system was replaced by a multi-stage cooling to approximate a continuous cooling. The temperature profile of the cooling stages is crucial to control the supersaturation level, which directs the crystallization process.
In this diploma project a solid understanding of the involved processes during the crystallization in the reactor is based on theoretical and experimental methods:

In the first stage, the experimental setup is simulated by using MatLab®. In these investigations, all parameters such as the mass ratio, the temperatures of the mixed feed streams, the seed particle size or the temperature profile of the waterbaths can be varied and modeled. These parameters directly influence the supersaturation in the system and therefore the crystal growth. The goal of this optimization is the increase in particle growth by taking the possibilities and limitations of the given experimental setup into account.

The second focus in this work is to prove the adaptability of the optimized process to another testing substance. From several possible substances, acetaminophen (Paracetamol, PAC) was chosen because of its chemical properties, commercial relevance and easy availability.
Although the mean retention time for PAC is equal to the experiments with ASA; process parameters like mass ratios and temperatures of the entering streams and the temperature profile of the cooling steps have to be established. Therefore, the MatLab® program is adapted to the solubility behavior of PAC and then used to simulate the process.
Similar to the experiments with ASA, the influence of the retention time on the crystal growth is to be investigated.
Finally the simulation results are carefully compared to the experimental results.

During the simulation, some simplificating assumptions are made (i.e. the assumption of a single seed particle size as well as the negation of nucleation agglomeration or breakage). The comparison of simulated and experimental results is essential for the understanding of the process of crystallization in the reactor and allows a more detailed definition of possible interferences.

2. SET-UP

2.1. PROCESS DESIGN

In a continuous tubular crystallizer, the growth of crystals is investigated. The apparatus consists of a feed solution stream and a seed suspension stream, which both are pumped separately by two peristaltic pumps and then mixed in a Y-branch. Subsequently, the mixed stream enters the reacting zone, consisting of a 15 m long, coiled tube with an inner diameter of 2 mm. The crystallizer is cooled by five waterbaths with decreasing temperatures to facilitate a constant supersaturation, which is the main reason for crystal growth. The chosen dimensions of the tubing allow a large surface-to-volume ratio and therefore easy removing of crystallization heat and cooling as well as a narrow residence time distribution. Therefore, a narrow particle size distribution (PSD) and good product quality can be expected.
Figure 2-1 shows the general set-up for the crystallization process.

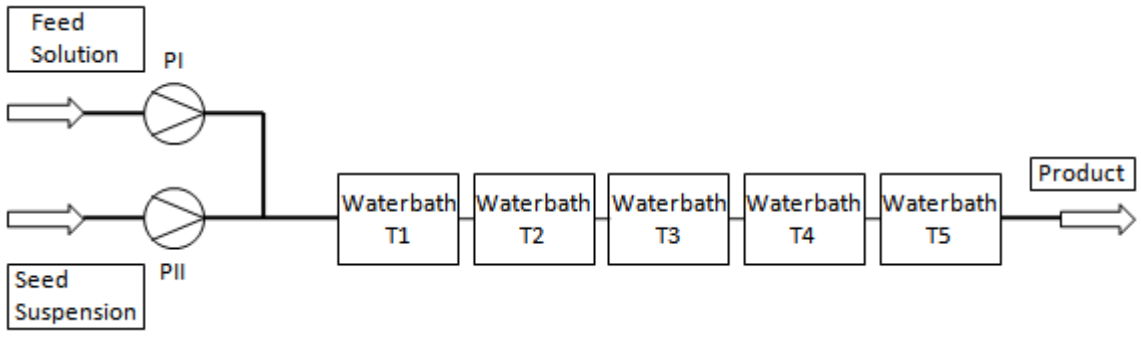

Figure 2-1: general set-up of the crystallization reactor

The same process design is implemented in MatLab® to simulate the experiments, providing that sampling only takes place in the experimental investigation.
The MatLab® simulation allows facile modeling of the process in a short time and without experimental errors. Nevertheless, a simulation can only work with assumptions and simplifications and can only reflect a small part of the overall situation.

The modeling substances for crystal growth are acetylsalicylic acid (ASA) and acetaminophen (PAC), both crystallized from ethanol (EtOH).
The process conditions like concentration of feed solution and seed suspension, preheating and cooling trajectory have to be adapted to the different solubility behavior of these substances. The flow rates of the two streams and thus the retention time were kept the same. Three various retention times were investigated in this diploma thesis in order to a gain comprehensive overview.

2.2. MATERIALS

crystallized material:		
acetylsalicylic acid	GL PHARMA	M = 180,16 g/mol
acetaminophen (paracetamol)	ALDRICH	M = 151,16 g/mol
solvent:		
ethanol	ROTH	99,8%, 1% MEK; M = 46,07 g/mol

The seed loading as well as the feed concentration for ASA were calculated using the Nývlt Equation (Maia et al., 2008 [5]), where x^* is the molar fraction of ASA at solubility equilibrium [mol_{ASA}/mol_{EtOH}] and the T in [K]. The parameters in Eq. 5 are:

N_1: 27,769
N_2: -2500,906
N_3: -8,323

$$\log(x^*) = N_1 + \frac{N_2}{T} + N_3 * \log(T) \qquad \textbf{Eq. 5}$$

For PAC data from Rasmuson, 2002 [19], Mazzotti, 2004 [14] and Méndez del Río and Rousseau, 2006 [11] are used. Méndez del Río and Rousseau derived Eq. 6 by using a van't Hoff fit on data by Granberg and Rasmuson [23]:

$$\ln(x^*) = \frac{-1836{,}8}{T} + 3{,}3078 \qquad \textbf{Eq. 6}$$

Figure 2-2 shows a comparison of the solubility equilibria of isobutyl propanoic phenolic acid (ibuprofen, IBU), acetylsalicylic acid (ASA) and acetaminophen (paracetamol, PAC), calculated and adapted by the above-named literature.

Ibuprofen could have been interesting as another model substance, but in a small series of preliminary experiments this substance proved to be difficult to handle. Furthermore, the very high solubility would have led to a considerably large consumption of material.

Therefore, paracetamol was chosen as a second test substance.

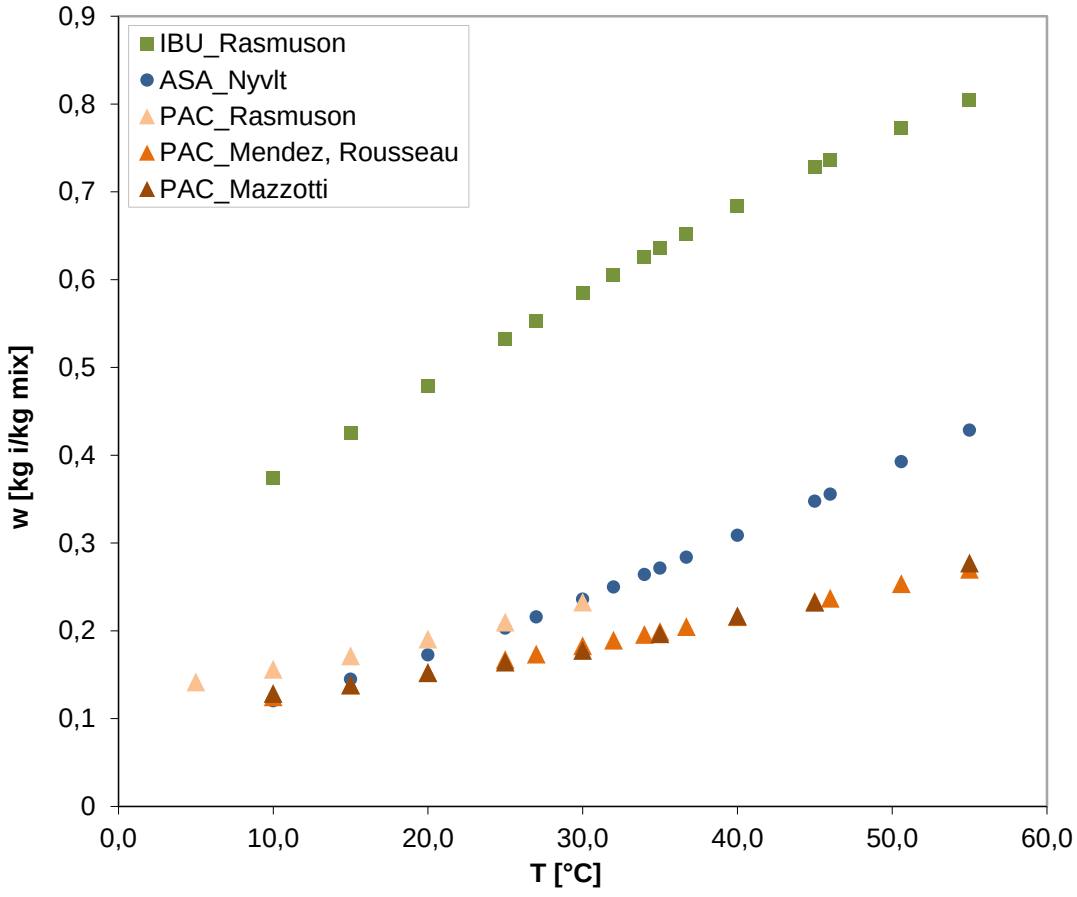

Figure 2-2: solubility of ASA, PAC and IBU

2.3. EQUIPMENT

preparing of seeds, storage vessel:

Name	Company/Specification
magnetic stirrer	IKAMAG RCT
stir bar	
bottle	SCOTT DURAN 1000 ml
scale	SARTORIUS

seed suspension:

Name	Company/Specification
PII (peristaltic pump)	ISMATEC Reglo Digital MS-2/6V 1.13C
tube	ID 1 mm, OD 3 mm (PTFE)
tube	PHARM MED ID 2.79 mm
stirrer	

feed solution:

Name	Company/Specification
PI (peristaltic pump)	ISMATEC BVP- Process IP 65 (3/6)
tube	PHARM MED ID 1.6 mm, OD 4.8 mm
stirrer	
waterbath	ULTRATERM P Selecta
waterbath	HAAKE D3

reactor:

Name	Company/Specification
T-junction	ID 2 mm (PTFE)
tube	ID 2 mm, OD 4 mm, length 15 m (Silicone)

cooling trajectory:

Name	Company/Specification
waterbath (2x)	LAUDA Alpha A24
waterbath	GRANT
waterbath	LAUDA 011
ultrasonic waterbath	ELMA TRANSONIC 35kHz
thermostat (3x)	LAUDA Alpha A24
thermostat	LAUDA E100

sampling:

Name	Company/Specification
silica frit, suction filter	
water jet pump	
vacuum pump	VACUUBRAND PC510
desiccator	

analysis:

Name	Company/Specification
QICPIC	SYMANTEC
analytical scale	METTLER AE200
microscope	LEICA DM 4000 M
microscope camera	LEICA DFC 290
thermometer (electric)	FLUKE 50 D

2.4. SET-UPS FOR BOTH MODEL SUBSTANCES AND THREE DIFFERENT RETENTION TIMES

According to previous experiments[2] the settings for ASA are:

Table 2-1: mass ratios and feed temperatures of ASA

	ASA [g]	EtOH [g]	T [°C]	T preheater [°C]
feed solution	300	600	62	40
seed suspension	250	500	25	-

The chosen values for PAC were derived from the settings for ASA in order to achieve similar supersaturation levels.

Therefore, the settings for PAC are:

Table 2-2: mass ratios and temperatures for PAC

	PAC [g]	EtOH [g]	T [°C]	T preheater [°C]
feed solution	185	500	65	55
seed suspension	250	500	25	-

The waterbath temperatures have been set to:

Table 2-3: temperatures of the cooling baths for ASA and PAC

	WB1 [°C]	WB2 [°C]	WB3 [°C]	WB4 [°C]	WB5 [°C]
ASA	34	31	27	22	18 (20)
PAC	43	39	34	28	22

To avoid blocking, some experiments of ASA have been repeated with a higher bath temperature of waterbath Nr. 5, hence 20 °C.

The pump settings are equal for both substances and set, according to the retention time, to:

Table 2-4: retention times and flow rates for ASA and PAC

retention time [s]	PI (feed solution) [ml/min]	PII (seed suspension) [ml/min]
164	13,4	3,8
124	17,8	5
112	19,7	5,5

Furthermore, seed particle sizes as measured during the experiments were set as a start value for the MatLab® simulation.

3. MODELS FOR SIMULATION IN MATLAB®

The models described in this chapter was developed for a recent publication of one of the IPPTs research groups and is adjusted to our problem.

The MatLab® calculation allows a prediction of the temperature profile, the product particle size, the supersaturation level and the dissolved ASA mass fraction during the crystallization process. To simplify the calculation, two major assumptions are made:

- The number of particles is constant. This means no agglomeration, breakage or nucleation during the process.
- The simulation does not deal with a particle size distribution. Therefore, all particles at a point x along the reactor have an identical particle size.

Further assumptions for the heat and mass balance of a tubular crystallizer (based on the requirements for a continuous block flow reactor) are:

- steady-state operating conditions
- constant density of the suspension
- no axial mixing
- a laminar, thermally fully developed flow, so no radial temperature and concentration gradient (ideal mixing)
- the particles and the liquid phase is defined as a suspension and have locally the same temperature
- constant heat transfer coefficient from suspension to the pipe and from the pipe to the ambient water as well as a constant heat conductivity through the pipe, thus a constant overall heat transfer coefficient
- the specific heat of crystallization is constant and equal to the negative value of the heat of fusion
- constant heat capacity of the suspension

The physicochemical properties for ASA and PAC, respectively and EtOH are listed in **Table** 3-1. The heat conductivity of the suspension, which is required in a later section, was set equal to the heat conductivity of pure EtOH.
The fusion enthalpy data refers to Maia, 2008 [5], Kirklin, 2000 [21] and the heat capacity of ASA refers to Maia, 2008 [5]. The heat capacity of PAC was set equal to ASA.

Table 3-1: properties of ASA, PAC and EtOH

	molar weight MW [kg/kmol]	density ρ [kg/m^3]	fusion enthalpy Δh_f [J/mol]	heat capacity c_p [J/kgK]	heat conductivity λ [W/mK]
ASA	180,16	1350	29800	1260	-
PAC	151,16	1290	29800	1260	-
EtOH	46,07	790	-	2400	0,1676

The characteristics of the crystallizer are listed in **Table 3-2**.

Table 3-2: characteristics of the crystallizer

length L [m]	inner diameter d_{inner} [m]	outer diameter d_{outer} [m]
15	0,002	0,004

heat conductivity λ_{tubing} [W/mK]	inner heat transfer coef. α_{inner} [W/m^{2}K]	outer heat transfer coef. α_{outer} [W/m^{2}K]
0,3	306	1494

The inner heat transfer coefficient is valid for a pipe like the used tubing and for EtOH at given conditions. The outer heat transfer coefficient was determined empirically by cooling of tempered EtOH and then calculated assuming a constant wall temperature and hence a constant Nusselt number (Nu) of 3,651 Kirklin, 2000 [21].

All other settings agree with data specified in chapter 2. The seed particle sizes were set according to the experiments and varied within a certain range to demonstrate the influence of the seed particle size (see also chapter 5).

3.1. BASIC EQUATIONS FOR CRYSTALLIZATION

Basic Calculations of the Seed Suspension:

The solid mass fraction in the seed suspension w_{solid} can be calculated from

$$w_{solid} = \frac{w_{seed} - w_{diss,seed}}{1 - w_{diss,seed}} \quad \textbf{Eq. 7}$$

Here, the total mass fraction w_{seed} is calculated from the mass of model substance and the mass of EtOH. The equilibrium mass fraction $w_{diss,seed}$ of model substance refers to the solubility of ASA and PAC in EtOH according to eq.3 and eq.4, respectively.

Basic Calculations of the Feed Solution (EtOH-Solution):

The mass fraction of dissolved substance in EtOH w_{EtOH} in the feed solution can be calculated with the mass of substance in the feed solution $m_{subst,EtOH}$ and the mass of EtOH in the feed solution $m_{EtOH,EtOH}$ from:

$$w_{EtOH} = \frac{m_{subst,EtOH}}{m_{subst,EtOH} + m_{EtOH,EtOH}} \quad \textbf{Eq. 8}$$

Material Balance in the Mixing Zone:

The mass fraction of solid substance $w_{solid,feed}$ in the mixing zone can be calculated from w_{solid} and the mass flow rate of seed suspension $\dot{m}_{seed}$ divided through the total feed mass flow rate $\dot{m}_{feed}$ as:

$$w_{solid,feed} = \frac{w_{solid} * \dot{m}_{seed}}{\dot{m}_{feed}} \quad \textbf{Eq. 9}$$

Here $\dot{m}_{feed}$ can be calculated as:

$$\dot{m}_{feed} = \dot{m}_{seed} + \dot{m}_{EtOH} \quad \textbf{Eq. 10}$$

$\dot{m}_{\boldsymbol{EtOH}}$ denotes the mass flow rate in the feed solution.

The mass fraction of dissolved substance $w_{diss,feed}$ can be calculated from the seed suspension properties and w_{EtOH} :

$$w_{diss,feed} = \frac{w_{diss,seed} * \dot{m}_{seed} * (1 - w_{solid}) + w_{EtOH} * \dot{m}_{EtOH}}{\dot{m}_{seed} * (1 - w_{solid})} \quad \textbf{Eq. 11}$$

Particle Concentration in the Reactor:

The particle concentration N_{conc} in the entering stream can be calculated from $w_{solid,feed}$ and the seed particle size $d_{p,seed}$ as:

$$N_{conc} = \frac{w_{solid,feed} * \rho_{feed}}{\frac{{d_{p,seed}}^3 * \pi}{6} * \rho_{subst}} \quad \textbf{Eq. 12}$$

Here, ρ_{feed} is the density of the entering stream, calculated from the volume flow rates of seed suspension $\dot{Q}_{seed}$ and feed solution $\dot{Q}_{EtOH}$ as:

$$\rho_{feed} = \frac{\dot{m}_{feed}}{\dot{Q}_{seed} + \dot{Q}_{EtOH}} \quad \textbf{Eq. 13}$$

Energy Balance Equation:

For calculating the energy balance, the heat transfer coefficient $k_{heat,tot}$ along the tubing is calculated from:

$$k_{heat,tot} = \frac{1}{\frac{d_{outer}}{2} * (\frac{1}{\frac{d_{inner}}{2} * \alpha_{inner}} + \frac{\ln\frac{d_{outer}}{d_{inner}}}{\lambda_{tubing}} + \frac{1}{\frac{d_{outer}}{2} * \alpha_{outer}})} \quad \textbf{Eq. 14}$$

The differential equation for the temperature profile is:

$$\frac{dT}{dx} = f_3 * (T(x) - T_{amb}) * f_4 * d_p(x)^2 * \frac{\frac{w_{diss}(x)}{\frac{1}{\rho_{EtOH}} + \frac{w_{diss}(x)}{\rho_{subst}}} - \rho_{subst,sat}(T)}{k_{heat,tot} * (T(x) - T_{amb}) - 1} \quad \textbf{Eq. 15}$$

Here, the constant factors f_3 and f_4 are:

$$f_3 = \frac{d_{outer} * \pi}{c_{p,seed} * m_{seed} + c_{p,EtOH} * m_{EtOH}} * k_{heat,tot} \quad \textbf{Eq. 16}$$

$$f_4 = \frac{N * F_{shape} * K_g * \Delta h_{crist}}{L * d_{outer}} \quad \textbf{Eq. 17}$$

$$N = N_{conc} * l * \frac{d_{inner}^2 * \pi}{4} \quad \textbf{Eq. 18}$$

In these equations $T(x)$ is the temperature profile along the tubing, T_{amb} is the ambient temperature according to the temperature of the waterbaths, $w_{diss}(x)$ is the dissolved model substance along the tubing, ρ_{EtOH} and ρ_{subst} are the densities of pure components and $\rho_{subst,sat}(T)$ denotes the partial saturation density of the model substance at temperature T.
The shape factor of the particles F_{shape} is assumed to be equal to unity. *N* is the number of particles, K_g is the mass transfer coefficient of the model substance in the EtOH solution and calculated as $1*10^{-5}$ m/s (Eder et al, 2010 [2]) and Δh_{crist} is the heat of crystallization, calculated as $30{,}2*10^6/MW_{subst}$ [J/kg] (Eder et al., 2010 [2]).

Mass Balance for the Dissolved Model Substance:

The mass balance equation for dissolved model substance is expressed by:

$$\frac{dw_{diss}}{dx} = -f_1 * d_p(x)^2 * \left(\frac{w_{diss}(x)}{\frac{1}{\rho_{EtOH}} + \frac{w_{diss}(x)}{\rho_{subst}}} - \rho_{subst,sat}(T) \right) \qquad \textbf{Eq. 19}$$

The constant factor f_1 is:

$$f_1 = \frac{1}{\dot{m}_{EtOH,feed}} * \frac{N * F_{shape} * K_g * \pi}{l} \qquad \textbf{Eq. 20}$$

$\dot{m}_{EtOH,feed}$ denotes the mass flow of pure EtOH in the entering stream.

Mass Balance Equation for Solid Model Substance:

Provided breakage and agglomeration are neglected, the differential equation for the evolution of the particle diameter along the tubing can be calculated as:

$$\frac{d(d_p)}{dx} = f_2 * \left(\frac{w_{diss}(x)}{\frac{1}{\rho_{EtOH}} + \frac{w_{diss}(x)}{\rho_{subst}}} - \rho_{subst,sat}(T) \right) \quad \textbf{Eq. 21}$$

where d_p denotes the particle diameter.

The constant factor f_2 is:

$$f_2 = \frac{2 * F_{shape} * K_g * \frac{d_{inner}^2 * \pi}{4}}{\left(\dot{Q}_{seed} + \dot{Q}_{EtOH}\right) * \rho_{subst}} \quad \textbf{Eq. 22}$$

4. EXPERIMENTAL DESIGN

4.1. PREPARATION OF SEED SUSPENSION AND FEED SOLUTION

For the experiments with ASA, to prepare the seed suspension 250 g of ASA and 500 g of EtOH were weighted into a 1000 ml bottle. The mixture was stirred with a stir bar on a magnetic stirrer for at least 24 h at room temperature to reach the equilibrium. The size and shape of the developed seeds is affected by mechanical effects like particle-particle and impeller-particle collisions. Thus, the crystals were mainly formed by breakage and friction. Although the preparing procedure was always kept constant, the mean seed size of all experiments varied between 100 and 190 µm (the overall seed size in one sample even ranged from 10 to 400 µm).
The feed solution were prepared by weighting ASA (300 g) and EtOH (600 g) in a round bottom flask, heating it up to 62 °C and while stirring until the ASA was completely dissolved.

The preparation of the PAC seed suspension was the same as for ASA. Due to the altered solubility properties, the feed solution was prepared by dissolving PAC (185 g) in EtOH (500 g), upon heating to 65 °C.

4.2. EXPERIMENTAL PROCEDURE

Before each run the pumps were calibrated. In order to determine the volume flow, the mass of EtOH at 20 °C (density of EtOH at 20 °C: 790 kg/m^3), which was furnished in 1 min, was determined.

Subsequently the reactor was flushed with warm EtOH to clean the tubing from residues from previous experiments by pumping the liquid only with PI. During this cleaning period, a seed sample was taken as described in chapter 4.3.

Hence, the seed suspension stream was connected to the Y-branch and pumped in the reactor together with pure EtOH in order to ensure the presence of seeds in the Y-branch. The absence of solid particles led to nucleation and thereby to blocking in previous experiments both in the Y-branch and the reactor.

Then both pumps were stopped simultaneously and the feed stream was switched from pure EtOH to the feed solution. Now the experiment was started by switching on the pumps again and merging seed suspension and feed solution in the reactor. Before connecting the Y-branch to the reactor, the temperature of the mixed stream was recorded.

The reactor was coiled in five parts on a pipe (d = 0,1 m) of galvanized grid to enable a constant heat removal in the waterbaths.

Figure 4-1 shows a scheme of the build-up of the experiment. The crystallization started immediately in the mixing zone and crystals grew along the tubing.

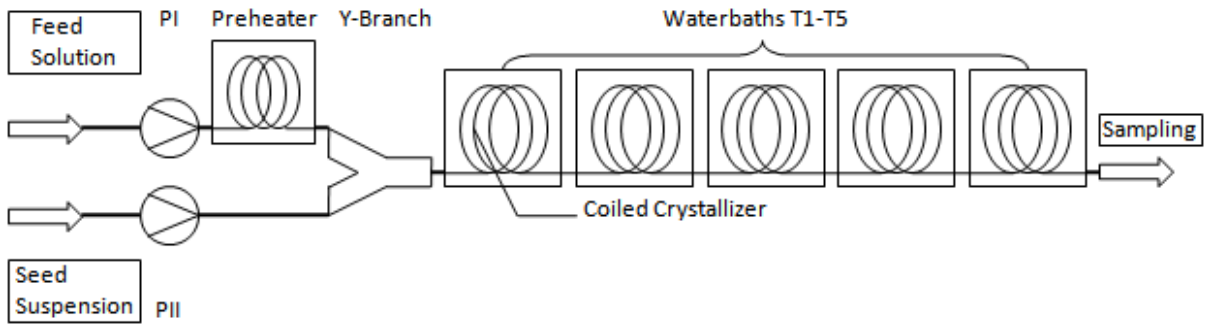

Figure 4-1: scheme of the experimental build-up

After ca. 2 min the first crystals passed the crystallizer and reached the end of the tubing. The literature points out steady-state conditions after five times the retention time. Thus, 10 min after starting the process the first, and 5 min later the second sample was taken.
The seed samples were taken before the seed suspension stream was entering the Y-branch, the product samples on the other hand at the end of the crystallizer. Finally, the temperature at the end of the reactor was measured and a second seed sample was taken. To conclude the experiment, the reactor was again flushed with EtOH to stop the crystallization and clean the system.

4.3. SAMPLING

For every run two seed samples were taken before entering the Y-branch, one before starting the process and the second one after finishing the crystallization to characterize the seeds and the constant seed quality. The two product samples served for the determination of crystal growth, particle shape and mass gain. In order to collect enough sample volume for the characterization, seed samples were taken over a period of 2 min, product samples for 1 min, respectively.
The sample stream was fed into a silica frit and filtered under applied vacuum. The crystals were washed with cyclohexane to prevent agglomeration and displace the saturated solution. Then the samples were stored in a desiccator and dried under vacuum.
The filtrate was weighted and then the EtOH was evaporated in a drying oven at 90 °C.

4.4. SAMPLE CHARACTERIZATION

To calculate the mass gain of the seed particles, the collected crystals and the filtrate were cooled and weighted, which allowed the establishment of a mass balance.
To determine the particle size, a part of the sample was analyzed by QICPIC. With the material available we could perform at least four repetitions.

In addition, pictures of the seed and product crystals were taken by microscope to investigate the shape of the crystals and evaluate interferences like breakage, nucleation or agglomeration.

5. SIMULATION RESULTS

5.1. PROFILES OF TEMPERATURE, PARTICLE SIZE OF PRODUCTS AND SUPERSATURATION VERSUS LENGTH

The settings for the ASA simulation are summarized in **Table 5-1**. To optimize the cooling process which allows in the beginning a slight and in the end a strong cooling, the temperature steps get bigger from bath to bath. The mass ratio of ASA/EtOH and the seed particle size agree to previous experimental data.

The simulation does not include nucleation, agglomeration nor intergrowth and abrasion of crystals. Furthermore the mean crystal size of seeds is set at an average diameter. The simulation is only valid for a batch of particles which have exactly the same size and does not consider the particle size distributions.

Table 5-1: settings for ASA simulation

ASA		T Waterbaths		34-31-27-22-18	°C
	Feed	T Preheater		40	°C
		Mass	ASA	250	g
			EtOH	500	g
		PI		13,4	ml/min
	Seed	T		25	°C
		Mass	ASA	300	g
			EtOH	600	g
		PII		3,8	ml/min
		Seed Size		169	µm

For ASA the temperature profile starts at around 37 °C. This is the mixing temperature from feed and seed stream and depends slightly on the flow rate. **Figure 5-1** shows the steady-state conditions in every water bath. Clearly illustrates the rapid temperature drop in each cooling

section to reach a plateau corresponding to the bath temperature. [1] The same conditions are also realized at higher flow rates.

The seed particles undergo a continuous, almost linear growth, and do not show a direct relationship on the temperature profile. This is based on the fact, that with steeper temperature gradient the supersaturation is at least constant, and so is the crystal growth.

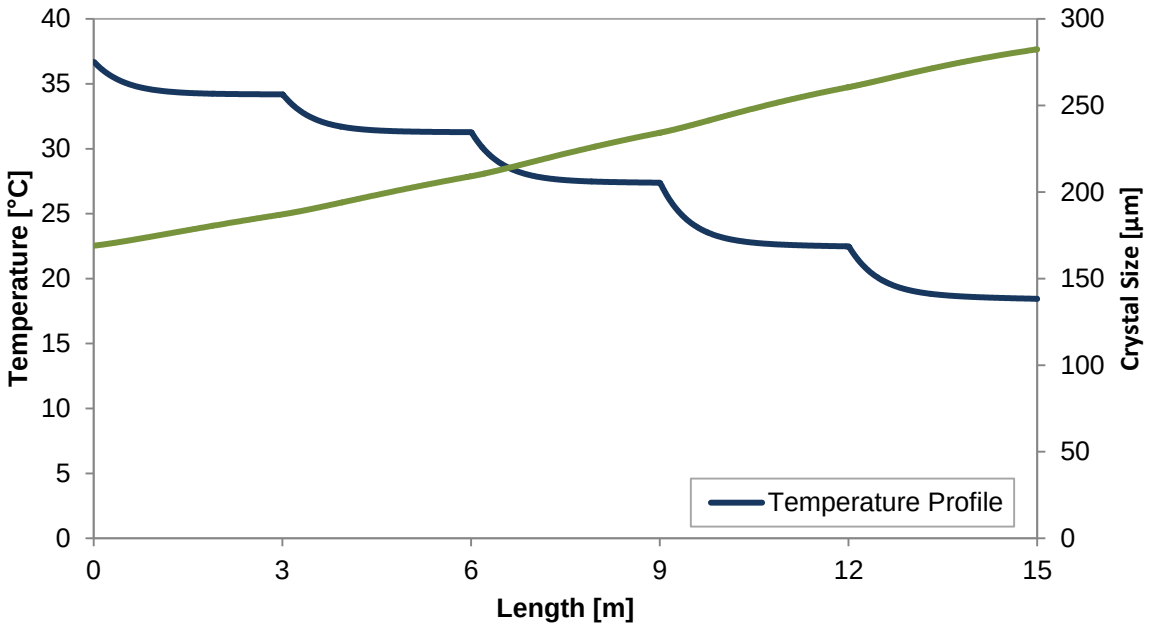

Figure 5-1: temperature profile and crystal growth of ASA

Figure 5-2 shows the solubility, the supersaturation and the dissolved ASA in the reactor.

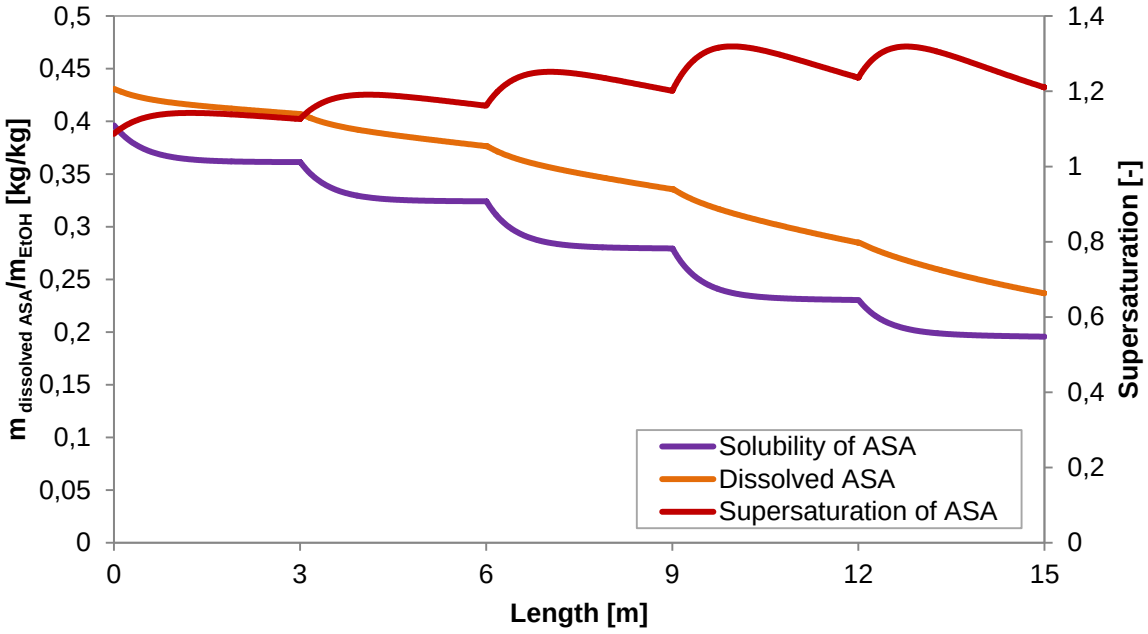

Figure 5-2: solubility, supersaturation and dissolved ASA

In the reactor, the solubility equals 0.4 kg dissolved ASA/kg EtOH at 37 °C at the reactor beginning and contains 0.9 kg dissolved ASA/kg EtOH at 18 °C at the reactor end, following the temperature profile. Every bath fulfills steady-state conditions. The supersaturation varies between 1.1 and 1.3. Due to the chosen bath temperature steps the maximum supersaturation increased slightly in each subsequent cooling section since the supersaturation was not consumed fast enough for the system to reach equilibrium conditions. However, this allowed fast crystal growth while supersaturation was still low enough to suppress nucleation. [1] In the initial stage of the water bath an abrupt temperature drop leads to an increased supersaturation. This effect may lead to blocking and therefore it has to be monitored during the experiments. The amount of dissolved ASA is always higher than the solubility of ASA to guarantee supersaturation. The concentration decreases along the reactor, because the molecules crystallize at the surface of the seed particles, which leads to particle size increases from 170 µm to 280 µm.

The simulation of the crystallization of PAC is based on the same assumptions as ASA, considering the different dependence of dissolution on the temperature (see
Figure 2-2: solubility of ASA, PAC and **IBU**

).

The settings for the simulation are summerized in **Table 5-2**.

Table 5-2: Settings for PAC simulation

PAC		T Waterbaths		43-39-34-28-22	°C
	Feed	T Preheater		55	°C
		Mass	PAC	185	g
			EtOH	500	g
		PI		13,4	ml/min
	Seed	T		25	°C
		Mass	ASA	300	g
			EtOH	600	g
		PII		3,8	ml/min
		Seed Size		83	µm

Because of the smaller temperature dependence of the dissolution of PAC, the mixing temperature at the inlet of the reactor has to be higher than in the experiments investigating ASA to allow a sufficient cooling distance and is around 48 °C. In spite of bigger cooling steps than for ASA, the steady-state conditions in every waterbath can be provided (**Figure 5-3**).

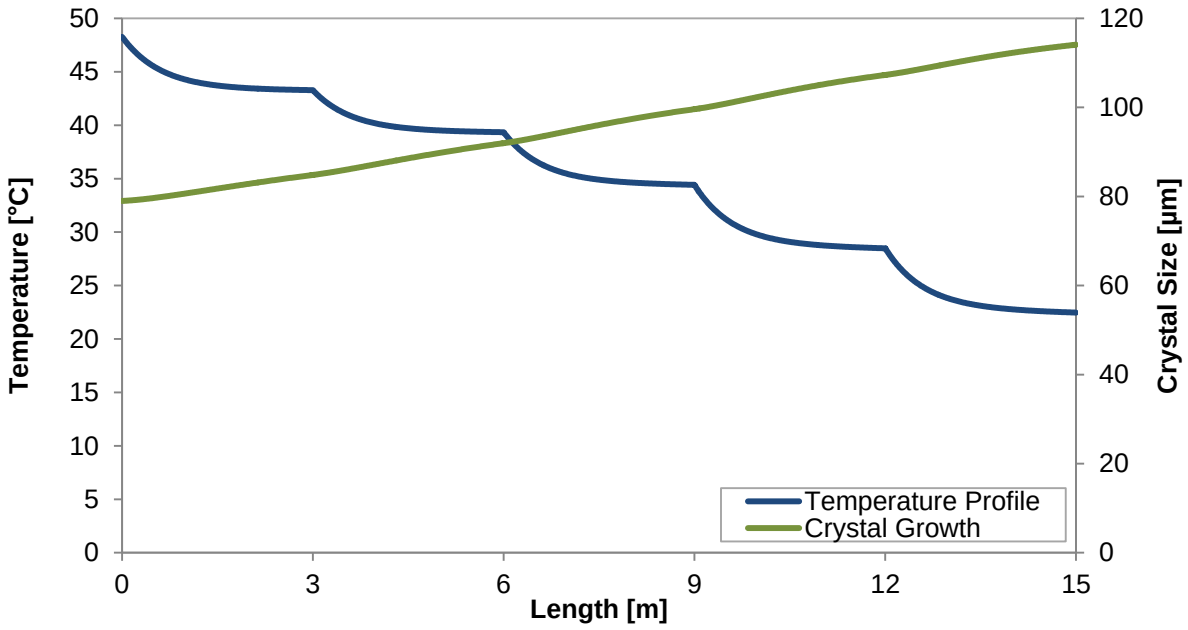

Figure 5-3: temperature profile and crystal growth of PAC

Contrary, the supersaturation of PAC (**Figure 5-4**) is lower than the supersaturation of ASA. This should be accepted to increase the material economy.

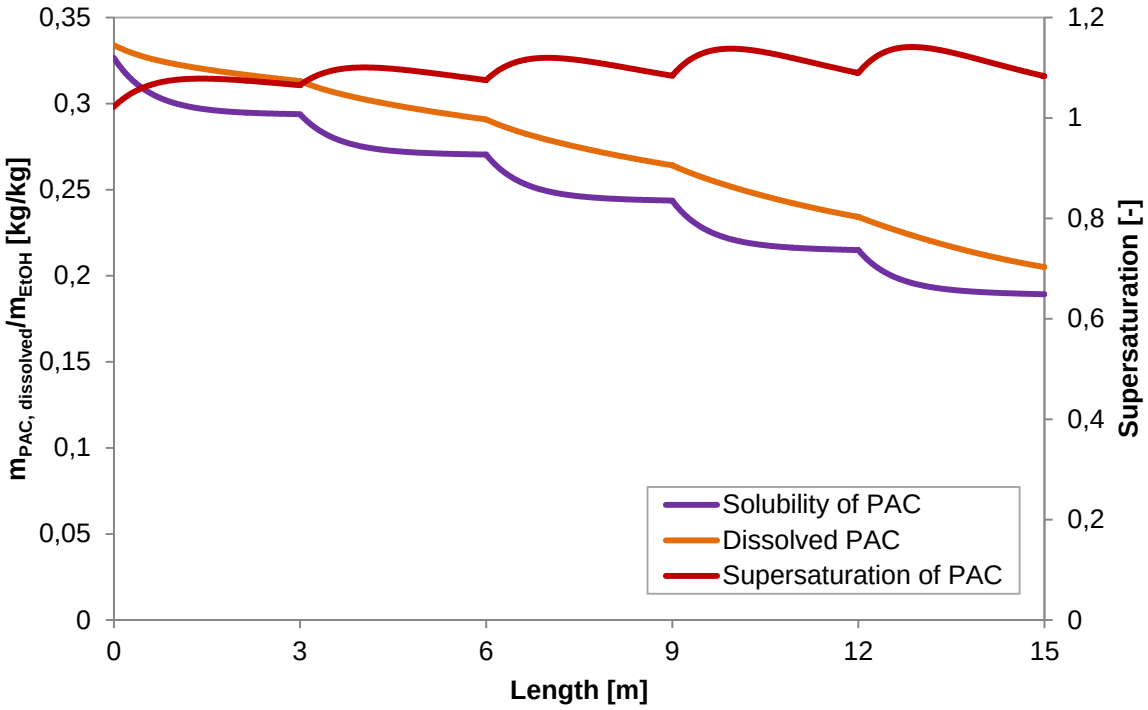

Figure 5-4: solubility, supersaturation and dissolved PAC

5.2. Dependence of Crystal Growth and Mass Gain versus Retention Time for Constant Seed Particle Size

In Figure 5-5 and Figure 5-6 the dependence of the seed crystal size and the retention time on the crystal growth for the modeling substance ASA and PAC, respectively, are shown. For a constant seed crystal size, the crystal growth increases according to the retention time. Clearly, the average crystal growth is a strong function of the retention time. [1] The simulation proves a logarithmic correlation, but for the investigated retention times a linear correlation is a valid approximation. At a constant retention time, larger particles undergo a more pronounced growth than smaller ones. Hence, the influence of the retention time on the crystal growth is distinct for larger crystals.

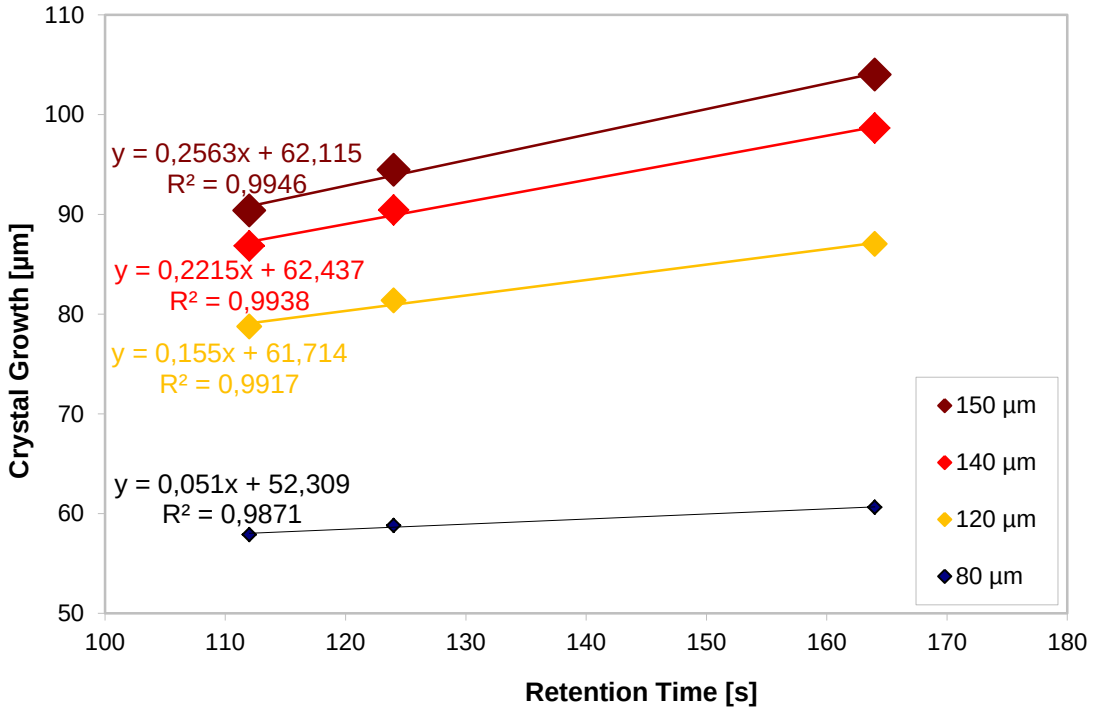

Figure 5-5: dependence of crystal growth of ASA

The crystal growth increases with increasing retention time and increasing seed size.

Shown in Figure 5-6, the simulation of PAC suggests a very small correlation between the crystal growth of seed particle sizes around 80 µm and the retention time. This effect was also observed during test runs in the CSCOTC and could lead to not significant experimental results.

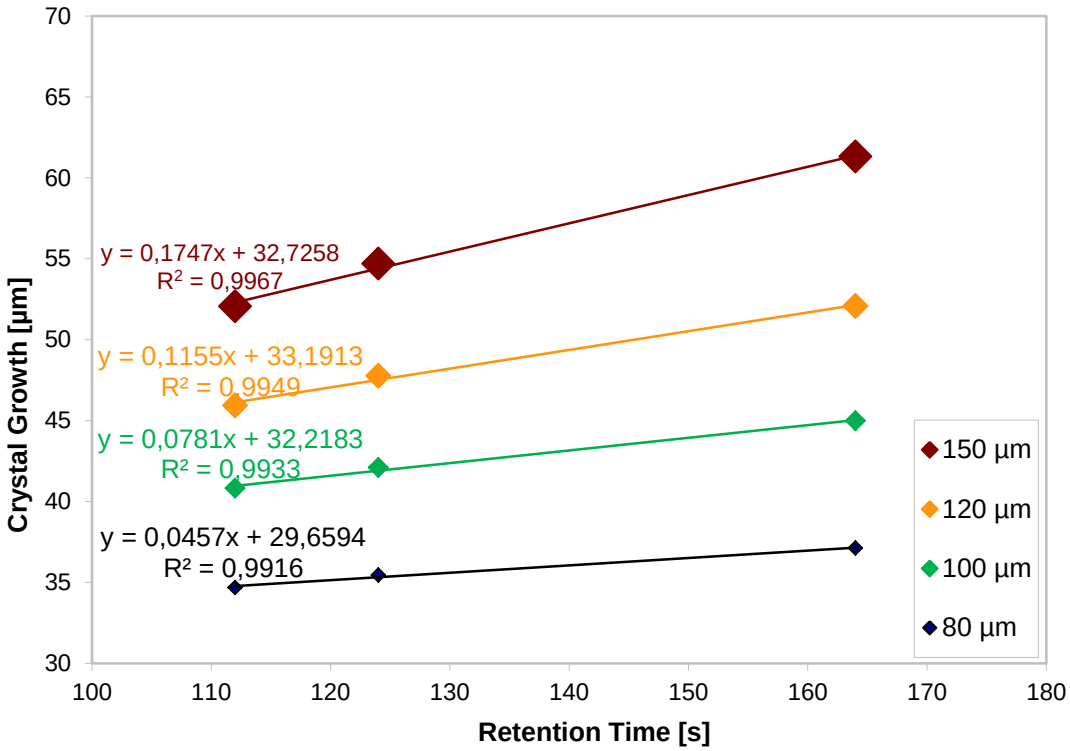

Figure 5-6: dependence of crystal growth of PAC

The crystal growth increases with increasing retention time and increasing seed size, although there is a minor influence of the retention time for small seed crystals

Furthermore, the influence of the retention time can be investigated by observing the achieved mass gain (see Figure 5-7 for ASA and Figure 5-8 for PAC, respectively). As a consequence of higher retention times, the mass gain increases. Both, the crystal growth as well as the mass gain are affected by the seed size. This effect decreases with increasing retention times. It is worth considering this effect because it gives information about the solubility behaviour depending on the crystal size.

The surface per mass is higher for small particles, so they allow even more molecules to crystallize on their surface. Due to this the mass gain increases with decreasing particle sizes. With high retention times there are only minor differences in mass gain. This can be traced back to the assumption that the retention time limits the crystallization. Thus, the seed particle size cannot be neglected. Based on the lower solubility of PAC, the mass gain is obviously lower than for ASA, even for equal seed particle sizes.

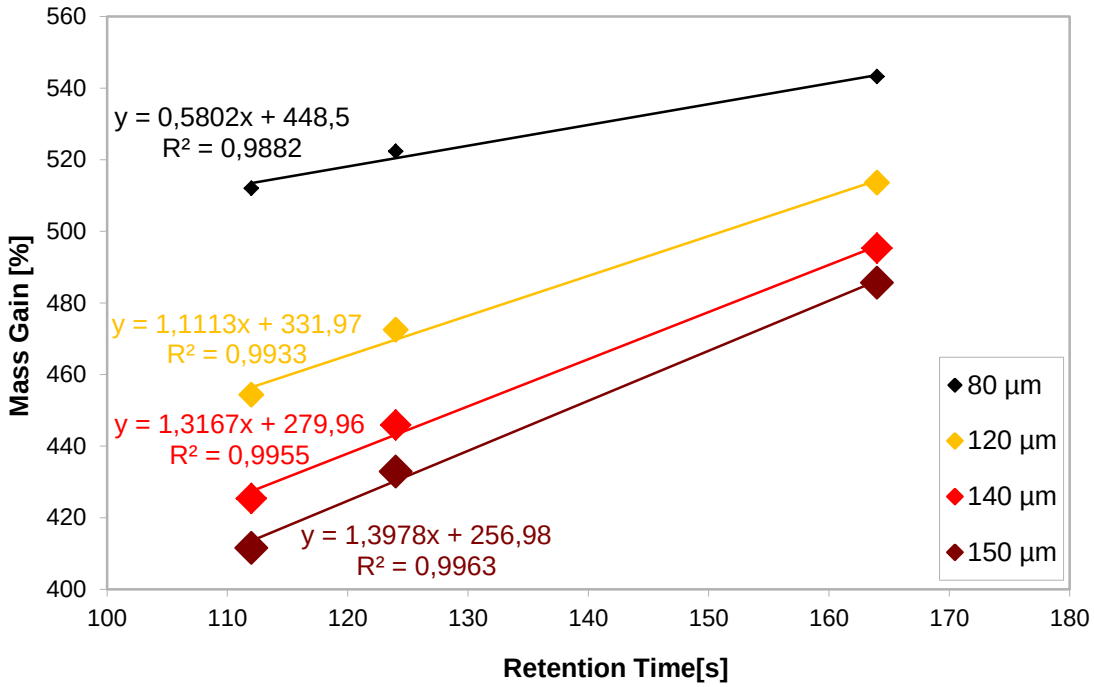

Figure 5-7: dependence of mass gain of ASA

The mass gain increases for smaller seed sizes due to the higher volume-to-mass ratio.

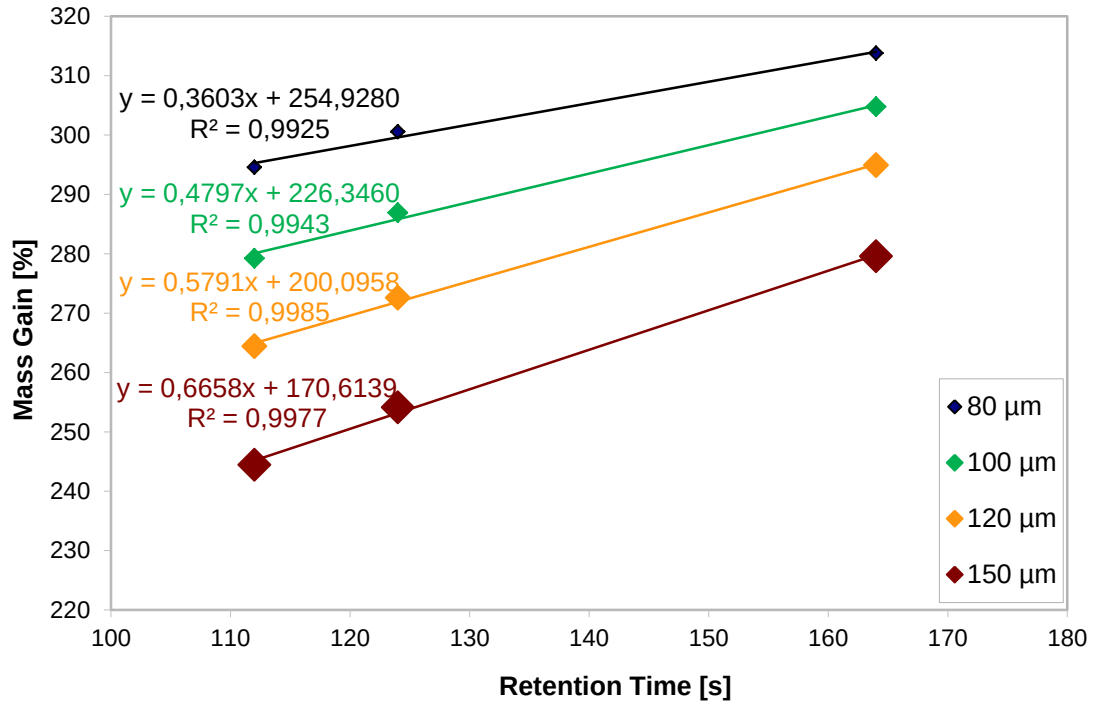

Figure 5-8: dependence of mass gain of PAC

The mass gain increases for smaller seed sizes due to the higher volume-to-mass ratio.

5.3. Dependence of Seed Particle Size versus Retention Time for Constant Crystal Growth and Constant Mass Gain

Obviously, the crystal growth is affected by the seed size and the retention time. Increasing seed sizes and increasing retention times cause a pronounced crystal growth and on the other hand, a decreased mass gain. The impact of the seed size is not as strong as the retention time, but should not be neglected. To accentuate this effect, a diagram for a constant crystal growth can be helpful.

As shown in **Figure 5-9** for ASA and **Figure 5-10** for PAC, increasing seed sizes result in the same crystal growth rates as higher retention times do. The growth of large particles shows a stronger dependence on the retention time than smaller particles do. In accordance to **Figure 5-9** for choosing equal retention times, an increase of the seed particle size of only 5 µm for small particles but 25 µm for big particles lead to the same crystal growth (80 µm and 110 µm, respectively). Therefore, the influence of the seed particle size is two times larger for large seed particles than for smaller ones. Due to this, to obtain the effect of the retention time, large seed crystals with a narrow PSD should be preferred. However, to control the crystal growth for a broad PSD by varying the retention time, small particles should be considered, because they are not as infected by the seed size than larger ones.

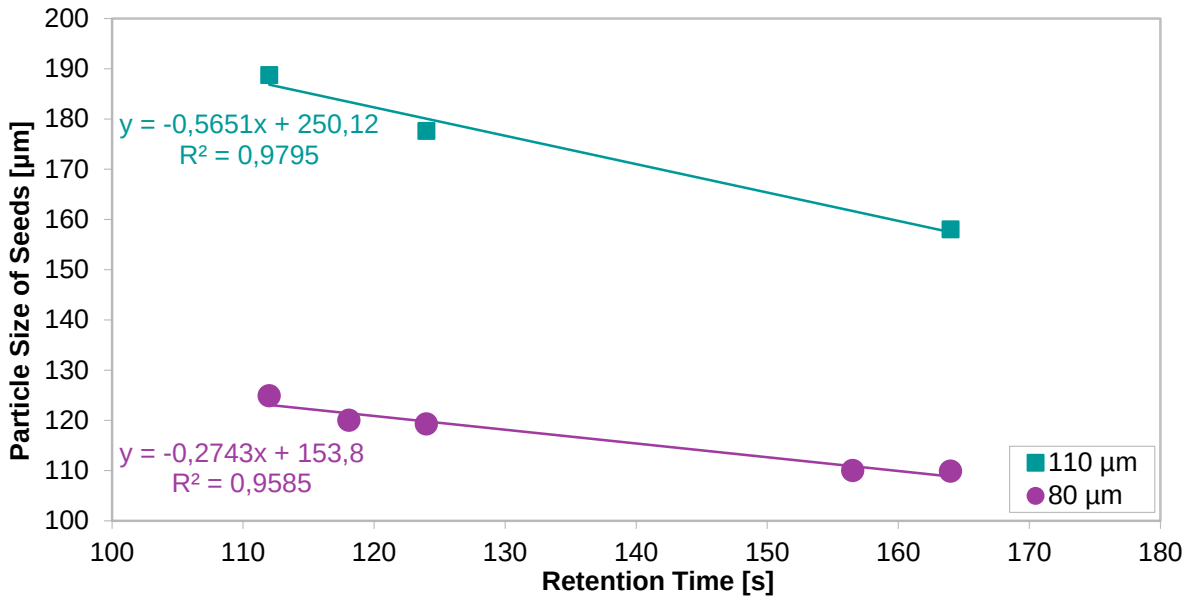

Figure 5-9: dependence of seed particle size vs. retention time of ASA

Both effects – retention time and seed size – can result in the same crystal growth. A narrow PSD should be preferred.

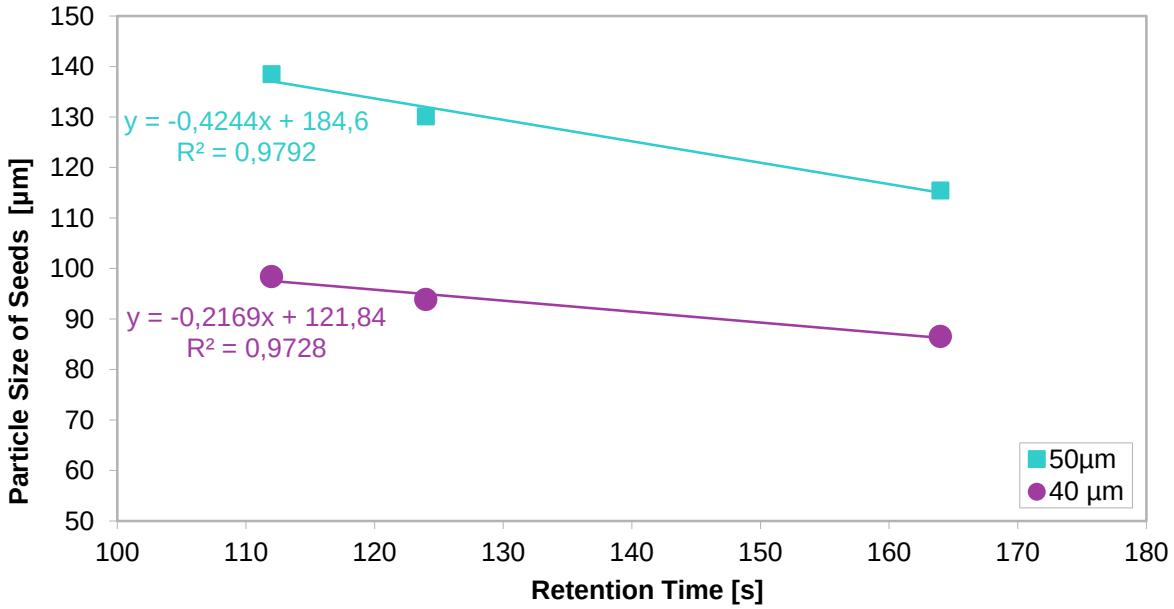

Figure 5-10: dependence of seed particle size vs. retention time for PAC

Both effects – retention time and seed size – can result in the same crystal growth. A narrow PSD should be preferred.

6. EXPERIMENTAL RESULTS

The aim of the experimental work was to compare and verify the simulated data to real reactions performed in the CSCOTC. Therefore the same temperature profile as in the simulation was achieved by counter-current cooled waterbaths. The weight of the washed and dried sample was measured to determine the mass gain and the PSD was analyzed by QICPIC. Moreover, to get a comprehensive idea of our crystals, we took pictures by microscope.

6.1. ASA

The optimized temperature profile of cooling allowed high crystal growth up to twice the seed particles diameter. This is in the range of previously measured data [2]. This success entails on the other hand a risk of blocking because of the average diameters of around 350 µm, which is 1/6 of the inner diameter of the tubing (2 mm). Especially the cooling drop in the last waterbath led to blocking in the experiments. The blocking is based on the too high supersaturation, which results in a rapid crystal growth and in secondary nucleation.

To avoid blocking, the last section of the tubing was pre-cooled in the waterbath T4 (22 °C) until steady-state-conditions have been reached. Afterwards the last section was taken back into the waterbath T5 (18 °C) for another two minutes until sampling. This procedure offered a much easier process control. Nevertheless, in case of blocking, the experiment has to be stopped and both pumps were switched to pure ethanol. All tubing sections were placed in an ultrasonic waterbath with 34 °C to dissolve the blockage. Subsequently, the experiment was restarted.

6.1.1. TABLES AND PSD

In **Table 6-1** the raw "process parameters", the settings for the pump PI (feed stream) and PII (seed-suspension) and the cooling watherbath temperatures (T1 to T5) are summarized. The raw "samples" shows the raw measurement data, whilst the raw "calculation" expresses the mass of seeds and products per minute and the volume mean diameter (VMD), respectively. Finally the raw "results" gives an overview about the mass gain calculated in percent of the seed mass and the crystal growth as a difference between the VMD of products and the VMD of seeds.

Table 6-1: ASA, retention time 164 s

Process parameters	pump settings	PI	13,4		PII	3,8		total flow 17,2		ml/min
	retention time							164		s
	waterbaths	T1	34	T2 31	T3	27	T4 22	T5	18	°C

ENr.	**100616-1**					
samples		1_{Seeds}	$2_{Product\ 1}$	$3_{Product\ 2}$	$4_{Seeds\ 2}$	
	t (sampling)	2	1	1	2	min
	mass	0,4704	2,5315	2,5057	0,455	g/min
	VMD	172,31	365,86	373,73	166,4	µm
calculation	m seed				0,2314	g/min
	m prod				2,5186	g/min
	VMD seed				169,355	µm
	VMD prod				369,795	µm
results	mass gain				1089	%
	crystal growth				200,44	µm
ENr.	**100630-2**					
samples		1_{Seeds}	$2_{Product\ 1}$	$3_{Product\ 2}$	$4_{Seeds\ 2}$	
	t (sampling)	2	1	1	2	min
	mass	0,6184	2,7484	2,8034	0,5958	g/min
	VMD	157,06	368,92	305,72	148,28	µm
calculation	m seed				0,3036	g/min
	m prod				2,7759	g/min
	VMD seed				152,67	µm
	VMD prod				337,32	µm
results	mass gain				914	%
	crystal growth				184,65	µm

Figure 6-1 shows the volume-density distribution $q_3(x)$ of two seed and two product samples for a retention time of 164 s. The expected crystal growth can be clearly demonstrated. Although we tried to avoid nucleation, the peak at 100 µm indicates a small amount of secondary nucleation. However, the steady-state conditions of the process have already been attained, evidenced by the very similar product sample distributions. The microscope pictures show the crystal growth as well as agglomeration and crystal intergrowth, which are existent but contribute only marginally to the volume increase.

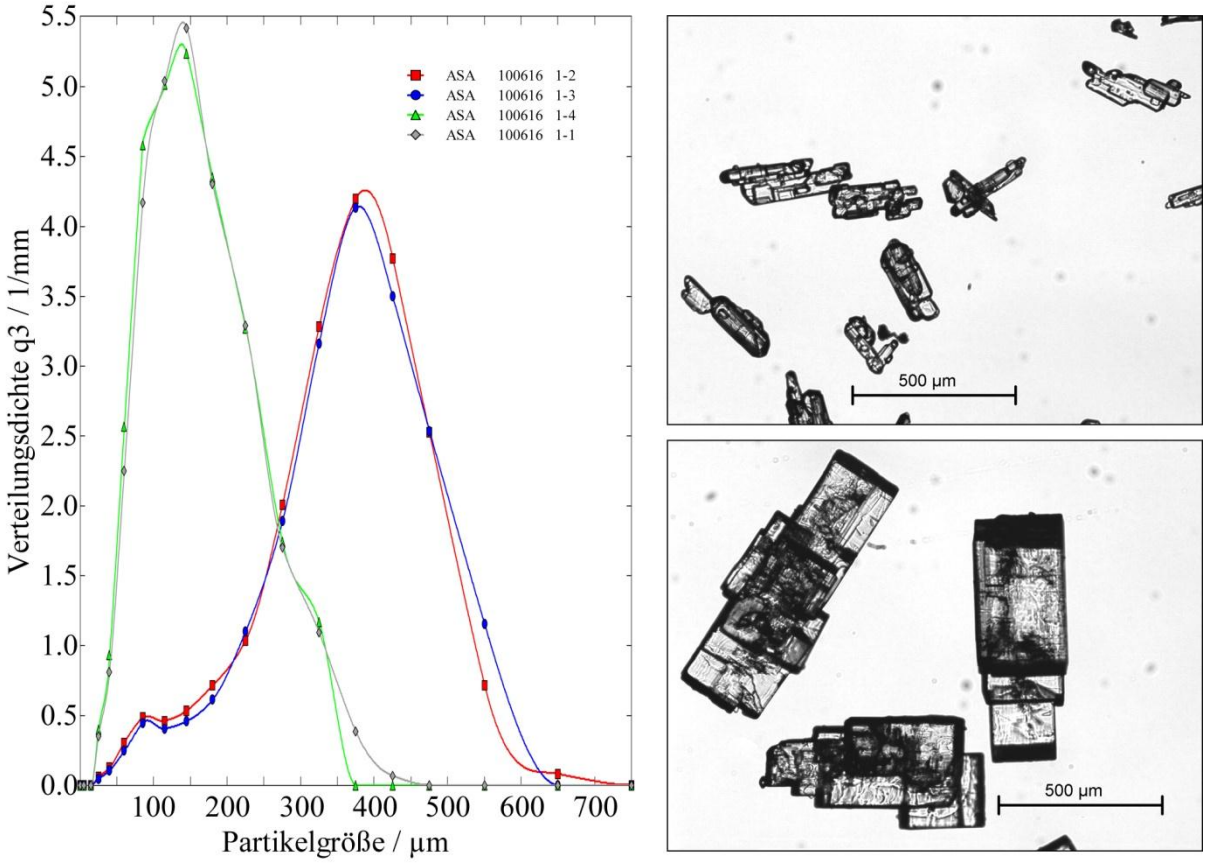

Figure 6-1: ASA, retention time 164 s, PSD, seed crystals, product crystals

Table 6-2 shows the process parameters and two experimental results for a retention time of 124 s. As expected, the crystal growth as well as the mass gain decreases due to shorter retention times.

Table 6-2: ASA, retention time 124 s

Process parameters	pump settings	PI	17,8		PII	5,0		total flow	22,8	ml/min
	retention time								124	s
	waterbaths	T1	34	T2 31	T3	27	T4 22	T5	18	°C

ENr.	**100623-1**					
samples		1_{Seeds}	$2_{Product\ 1}$	$3_{Product\ 2}$	$4_{Seeds\ 2}$	
	t (sampling)	2	1	1	2	min
	mass	1,0177	3,5057	3,4472	0,7282	g/min
	VMD	193,59	344,83	341,97	188,76	µm
calculation	m seed				0,4365	g/min
	m prod				3,4765	g/min
	VMD seed				191,175	µm
	VMD prod				343,4	µm
results	mass gain				796	%
	crystal growth				152,225	µm
ENr.	**100623-2**					
samples		1_{Seeds}	$2_{Product\ 1}$	$3_{Product\ 2}$	$4_{Seeds\ 2}$	
	t (sampling)	2	1	1	2	min
	mass	0,8684	3,2967	3,3726	0,8686	g/min
	VMD	184,69	350,4	344,94	178,74	µm
calculation	m seed				0,4343	g/min
	m prod				3,3347	g/min
	VMD seed				181,715	µm
	VMD prod				347,67	µm
results	mass gain				768	%
	crystal growth				165,955	µm

Similarly, **Figure 6-2** shows secondary nucleation. The microscope pictures evidence nicely shaped product crystals.

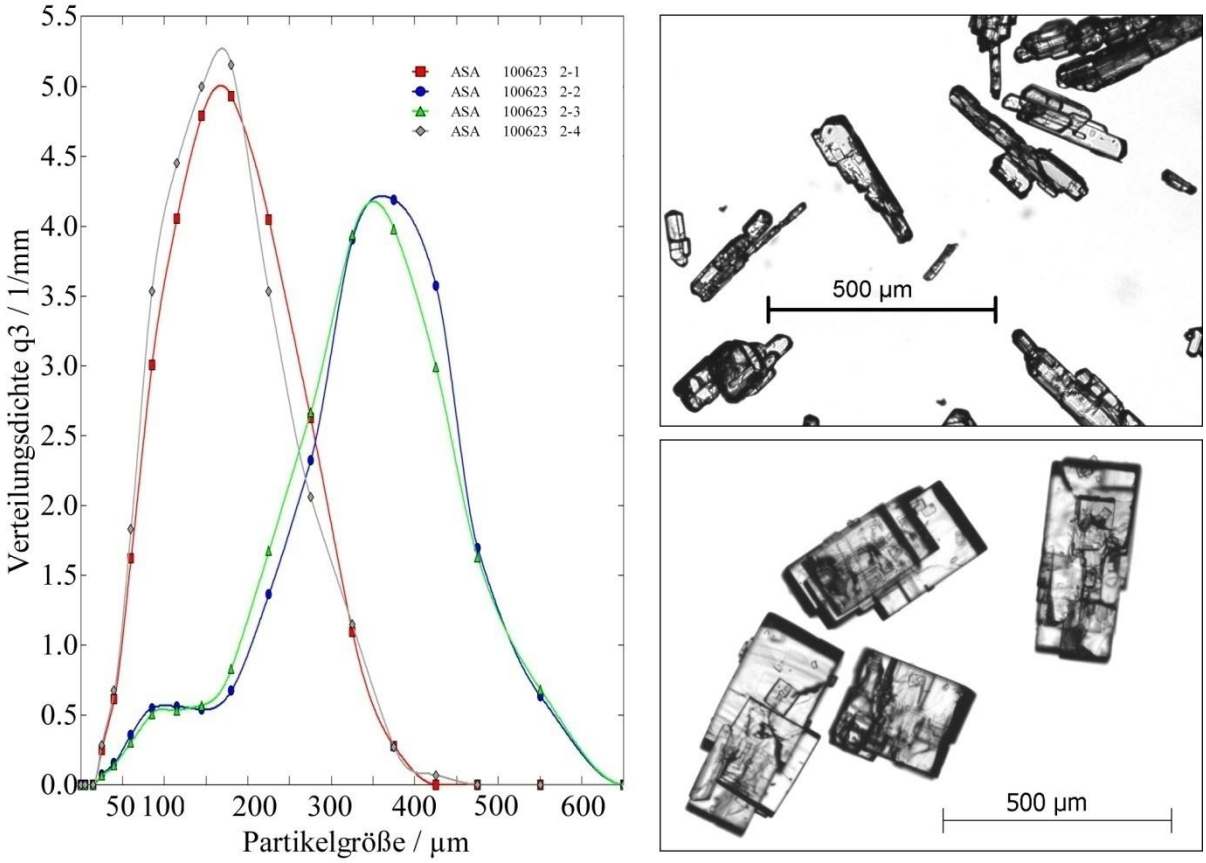

Figure 6-2: ASA, retention time 124 s, PSD, seed crystals, product crystals

Table 6-3 shows experimental data at a retention time of 112 s.

Table 6-3: ASA, retention time 112 s

Process parameters	pump settings	PI	19,7		PII	5,5		total flow	25,2	ml/min
	retention time								112	s
	waterbaths	T1	34	T2 31	T3	27	T4 22	T5	18	°C

ENr.	**100623-4**					
samples		1_{Seeds}	$2_{Product\ 1}$	$3_{Product\ 2}$	$4_{Seeds\ 2}$	
	t (sampling)	2	1	1	2	min
	mass	2,0336	4,944	4,8772	1,9858	g/min
	VMD	194,51	326,63	309,61	197,8	µm
calculation	m seed				1,0049	g/min
	m prod				4,9106	g/min
	VMD seed				196,155	µm
	VMD prod				318,12	µm
results	mass gain				489	%
	crystal growth				121,965	µm
ENr.	**100624-1**					
samples		1_{Seeds}	$2_{Product\ 1}$	$3_{Product\ 2}$	$4_{Seeds\ 2}$	
	t	2	1	1	1	min
	mass	2,1503	4,2092	3,8561	1,0983	g/min
	VMD	102,09	174,04	167,79	103,13	µm
calculation	m seed				1,0867	g/min
	m prod				4,0327	g/min
	VMD seed				102,61	µm
	VMD prod				170,915	µm
results	mass gain				371	%
	crystal growth				68,305	µm
ENr.	**100624-2**					
samples		1_{Seeds}	$2_{Product\ 1}$	$3_{Product\ 2}$	$4_{Seeds\ 2}$	
	t	1	1	1	1	min
	mass	1,0311	4,1676	4,2017	1,0963	g/min
	VMD	98,9	157,32	159,87	100,05	µm
calculation	m seed				1,0637	g/min
	m prod				4,1847	g/min
	VMD seed				99,475	µm
	VMD prod				158,595	µm
results	mass gain				393	%
	crystal growth				59,12	µm

To test the reproducibility of the results, experiments were repeated with a new batch of seed crystals. In this case it was necessary to produce a new charge of seed crystals. The seed crystal size of the experiments **100624-1** and **100624-2** is almost half than in experiment **100623-4**. This may be due to the fact that we used a charge of milled ASA. The procedure of preparing the seed suspension was not modified, notwithstanding the shape and size of seed particles have a strong dependence on the preparing procedure.
However, the experiments with less emerged seed particles demonstrate another influence on the crystal growth: the seed size. As explained in chapter 6, smaller seed sizes lead to reduced growth.

The decreased crystal growth due to low retention times and small seed particles is visible by the naked eye and even more cleareron the microscope pictures in **Figure 6-3**. The narrow PSD of product is an assumption for good product quality and is one of the aims of investigating a production process.

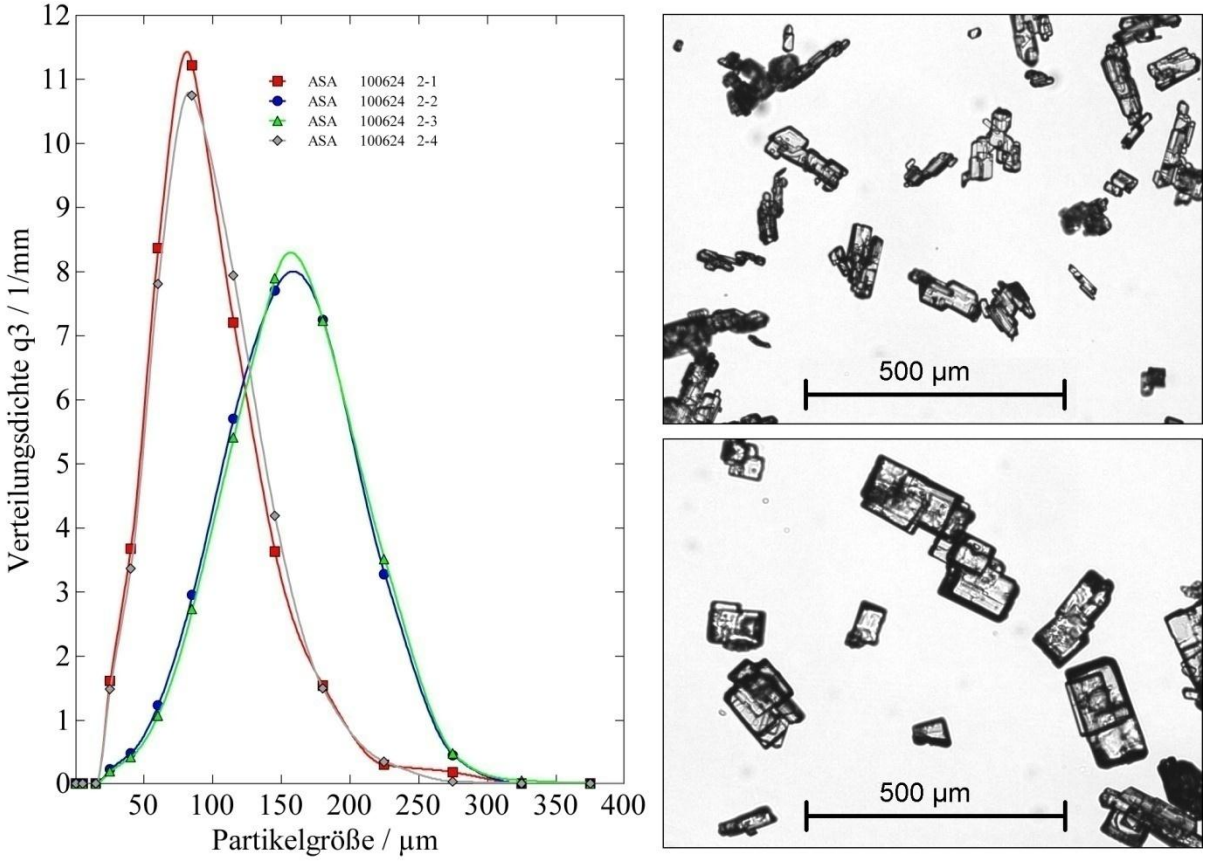

Figure 6-3: ASA, retention time 112 s, PSD, seed crystals, product crystals

Another possibility to control the blocking was to avoid the abrupt temperature drop in waterbath T5 by increasing its temperature to 20 °C. The respective data is listed in **Table 6-4**. This modification led to a smoothly operated process without blockage allowing two experiments to be run in sequence without interruption. The dependence of increasing crystal growth with increasing retention times could be demonstrated and is illustrated in **Figure 6-4**.

Table 6-4: ASA, various retention times for gentle cooling

Process parameters	pump settings	PI	13,4			PII	3,8			total flow 17,2	ml/min
	retention time									164	s
	waterbaths	T1	34	T2	31	T3	27	T4	22	T5 20	°C
ENr.	**100630-1**										
samples				1_{Seeds}		$2_{Product\ 1}$		$3_{Product\ 2}$		$4_{Seeds\ 2}$	
	t (sampling)			2		1		1		2	min
	mass			0,7209		2,7161		2,7153		0,6884	g/min
	VMD			155,22		324,8		324,86		158,75	µm
calculation	m seed									0,3523	g/min
	m prod									2,7157	g/min
	VMD seed									156,985	µm
	VMD prod									324,83	µm
results	mass gain									771	%
	crystal growth									167,845	µm

Process parameters	pump settings	PI	17,8			PII	5			total flow 22,8	ml/min
	retention time									124	s
	waterbaths	T1	34	T2	31	T3	27	T4	22	T5 20	°C
ENr.	**100630-3**										
samples				1_{Seeds}		$2_{Product\ 1}$		$3_{Product\ 2}$		$4_{Seeds\ 2}$	
	t (sampling)			2		1		1		2	min
	mass			1,1717		3,5531		3,5598		1,1708	g/min
	VMD			136,39		268,86		256,49		134,24	µm
calculation	m seed									0,5856	g/min
	m prod									3,5565	g/min
	VMD seed									135,315	µm
	VMD prod									262,675	µm
results	mass gain									607	%
	crystal growth									127,36	µm

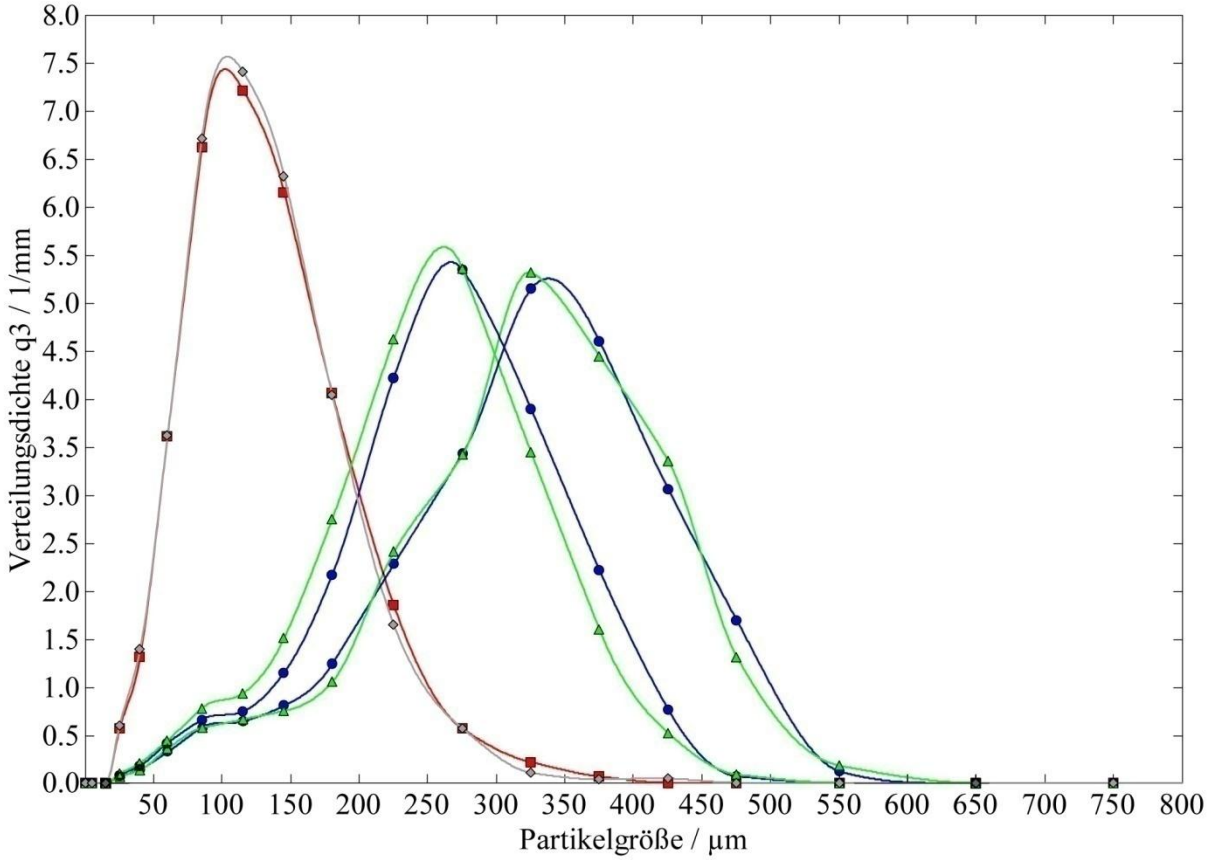

Figure 6-4: ASA, PSD of seeds and crystals for various retention times

6.1.2. COMPILATION OF RESULTS

A compilation of all experiments is helpful to illustrate the results. In the following diagram (**Figure 6-5**) the crystal growth is plotted against the retention time. The size of the diamonds gives an idea about the seed particle size. Additionally, smaller seed sizes are marked by lighter colors.

According to our expectation, the crystal growth increases with higher retention times. Furthermore, the larger seed size leads to a more pronounced crystal growth. This fact is also valid for the middle retention time, tough certain deviations are inevitable.

This may have different reasons. The major influence is probably the presence of secondary nucleation, which was neglected for the simulation. Also temporary fractional blockage of the

tubing, the classification of seeds in the supply vessel or local temperature deviations can influence the results. Moreover, sample splitting of dried crystals for the PSD-analysis can lead to deviations.

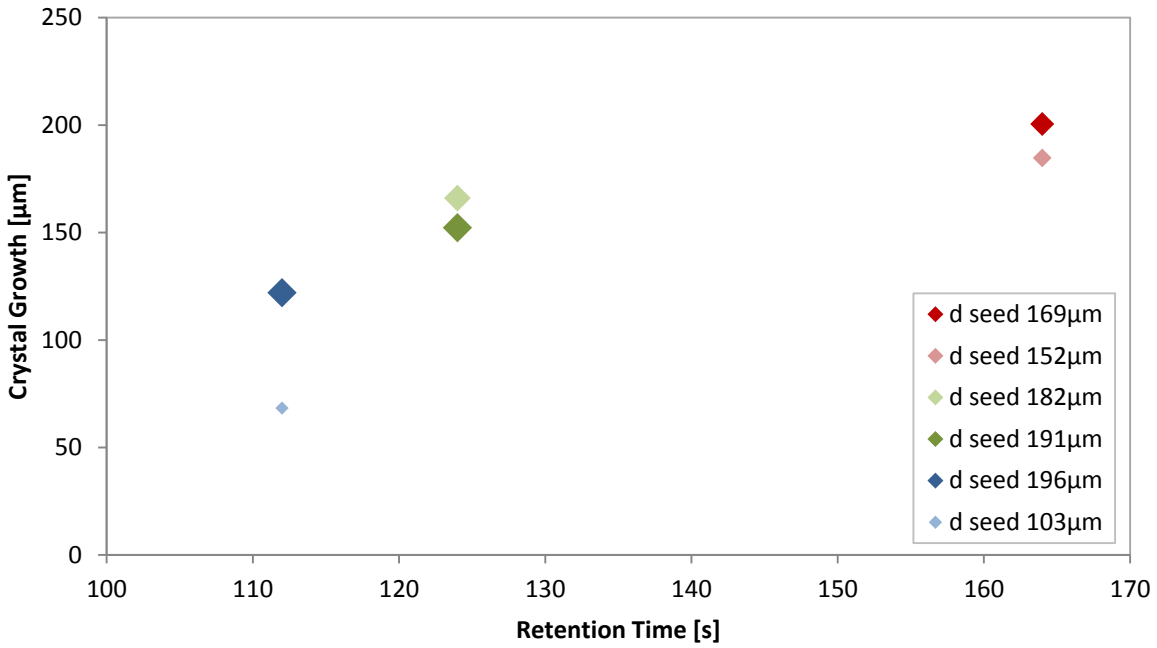

Figure 6-5: ASA, crystal growth for various retention times

Smaller and lighter colored diamonds mark smaller seed sizes. Larger seed particles and higher retention times lead to increased crystal growth.

Figure 6-6 shows the mass gain, in respect to their retention times. Similarly to the crystal growth, the increase in mass gain is directly proportional to the retention time. Most remarkably, that the seed crystal size influences the mass gain as well, although the simulation gave contrary results. This is justified in the assumption of "no nucleation" in the simulation.

The comparison of simulation versus experimental results is provided in chapter 7.

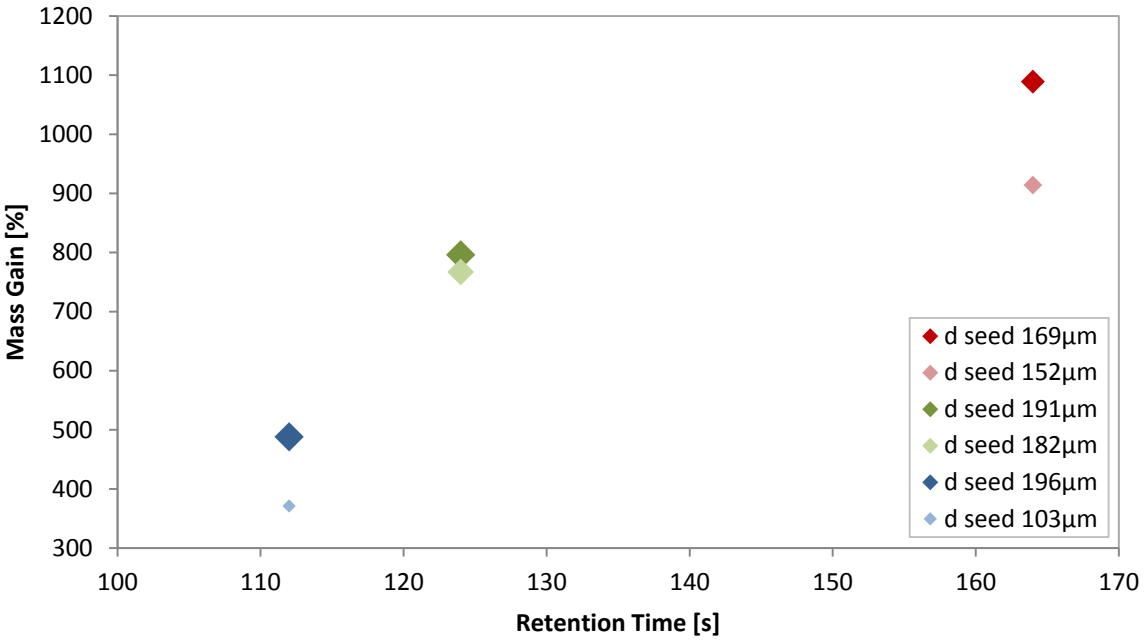

Figure 6-6: ASA, mass gain for various retention times

Smaller and lighter colored diamonds mark smaller seed crystals. The mass gain is directly proportional to the retention time.

6.1.3. FURTHER RESULTS

All experiments showed that nucleation cannot be neglected, but in two cases we found excessive secondary nucleation. As this was not the aim of this study, the results are listed separately.

Secondary nucleation can be effected by sudden cooling, absence of seed particles or high local supersaturation. The repeated occurrence of blocking necessitated the restart of the process. In two of these experiments, one of two samplings showed secondary nucleation.

Figure 6-7 and **Figure 6-8** show the volume-density distribution $q_3(x)$ and the microscopic pictures of two experiments. Nucleation is clearly indicated. The crystals have a well-defined cubic structure and an entirely different shape than conventionally produced seed crystals, which are exposed to high shear rates.

Based on these findings a detailed study of in-situ seed production could be developed.

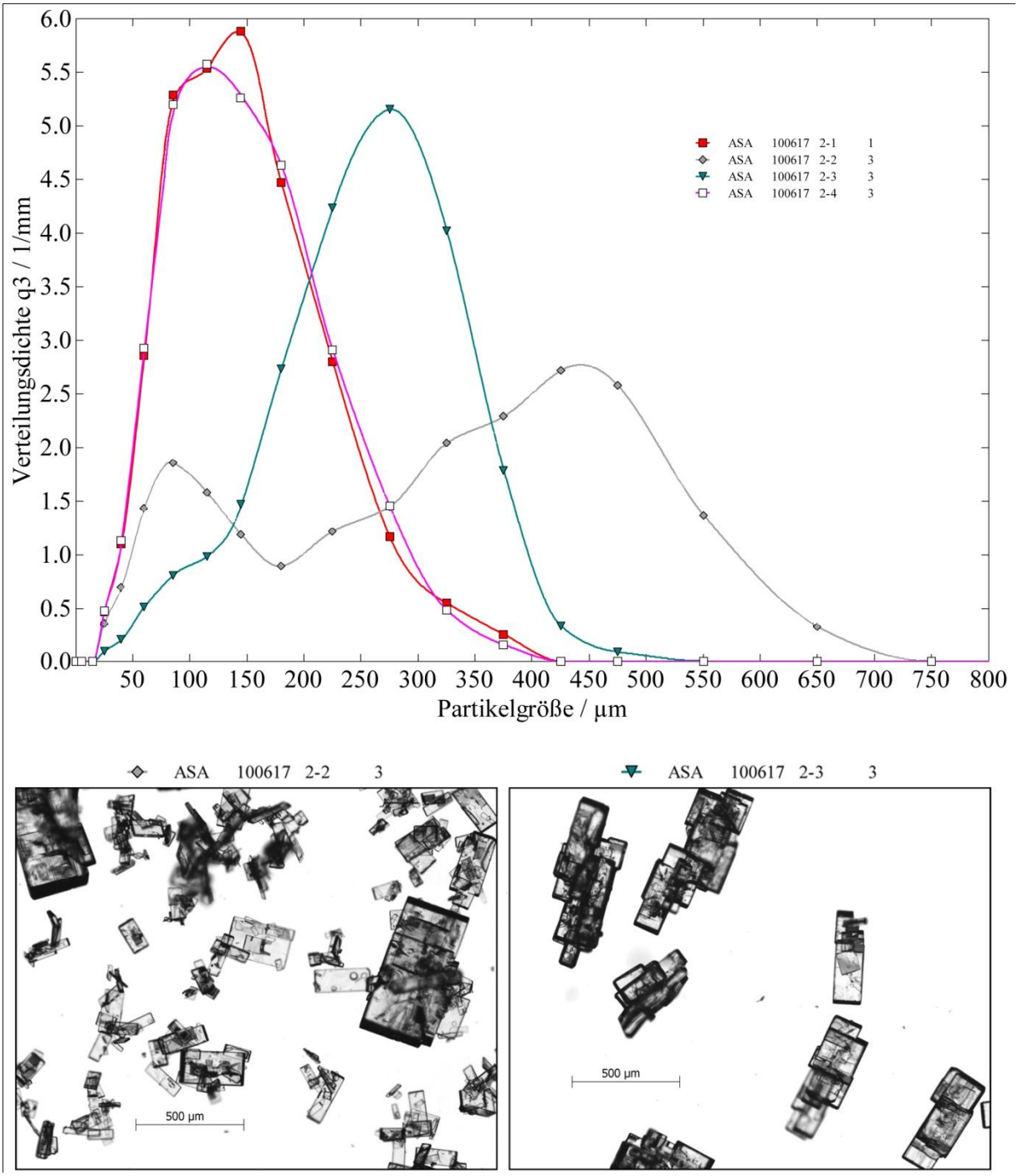

Figure 6-7: nucleation of ASA crystals during a retention time of 164 s

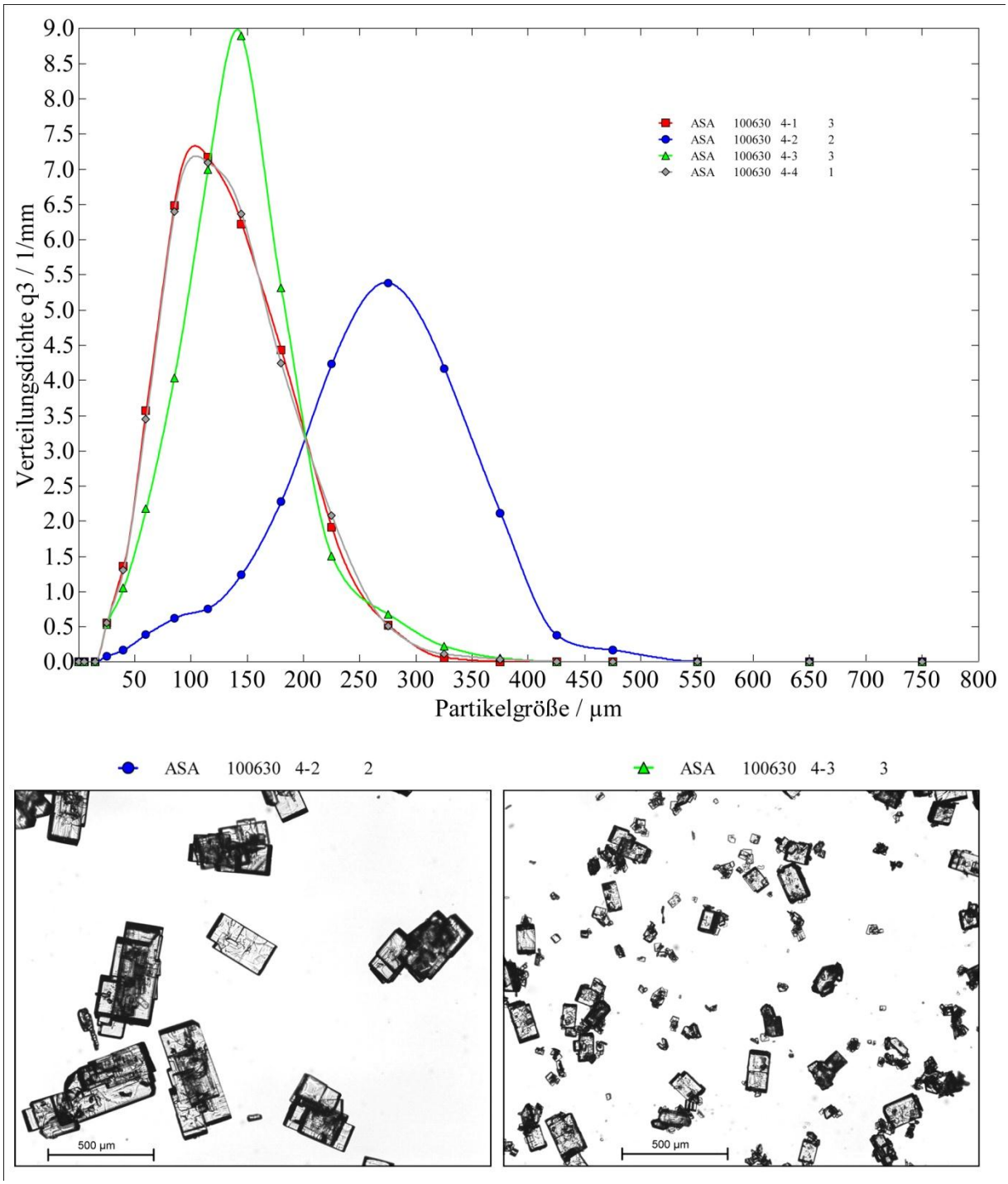

Figure 6-8: nucleation of ASA crystals during a retention time of 112 s

6.2. PAC

The aim of this experimental part was to investigate the adaptability of the tubular crystallizer to another crystallizable material such as paracetamol (PAC). It was essential to consider the different solubility behavior of PAC, which is reflected in a higher amount of dissolved PAC at the corresponding temperature, but a smaller gradient.
Hence, the supersaturation was not as high as in the experiments with ASA. The theoretical supersaturation of PAC ranged between 1.1 and 1.17.
Nevertheless, the seed particles had a smaller size and did not undergo an expressive growth, which allowed runs without any blockage. All experiments show a significant crystal growth and mass gain.

6.2.1. TABLES AND PSD

The pump settings and associated flow rates agree with ASA experiments, only the temperature drop has been adapted to the solubility behavior of PAC.
Table 6-5 gives an overview about the results at a retention time of 164 s. A significant increase in particle diameter could be obtained, which is mainly due to crystal growth and not to agglomeration. This fact is proved by the mass gain of product crystals.

Table 6-5: PAC, retention time 164 s

Process parameters	pump settings	PI	13,4			PII	3,8			total flow	17,2	ml/min
	retention time										164	s
	waterbaths	T1	43	T2	39	T3	34	T4	28	T5	22	°C

ENr.	**100624-4**					
samples		1_{Seeds}	$2_{Product\ 1}$	$3_{Product\ 2}$	$4_{Seeds\ 2}$	
	t (sampling)	2	1	1	2	min
	mass	1,2896	1,8582	1,8333	1,3009	g/min
	VMD	91,3	169,65	172,15	82,46	µm
calculation	m seed				0,6476	g/min
	m prod				1,8458	g/min
	VMD seed				86,88	µm
	VMD prod				170,9	µm
results	mass gain				285	%
	crystal growth				84,02	µm
ENr.	**100625-1**					
samples		1_{Seeds}	$2_{Product\ 1}$	$3_{Product\ 2}$	$4_{Seeds\ 2}$	
	t (sampling)	2	1	1	2	min
	mass	1,288	1,7645	1,9575	1,3021	g/min
	VMD	80,56	155,59	151,12	78,19	µm
calculation	m seed				0,6475	g/min
	m prod				1,8610	g/min
	VMD seed				79,375	µm
	VMD prod				153,355	µm
results	mass gain				287	%
	crystal growth				73,98	µm

Figure 6-9 shows the volume-density distribution $q_3(x)$ of one seed and two product samples for a retention time of 164 s. The expected crystal growth can be clearly demonstrated. The steady-state conditions of the process have already been attained, shown by the very similar distributions of the product samples. The microscope pictures show well-shaped cubic product crystals, as well as agglomeration and crystal intergrowth, which are partly responsible for the increase in volume.

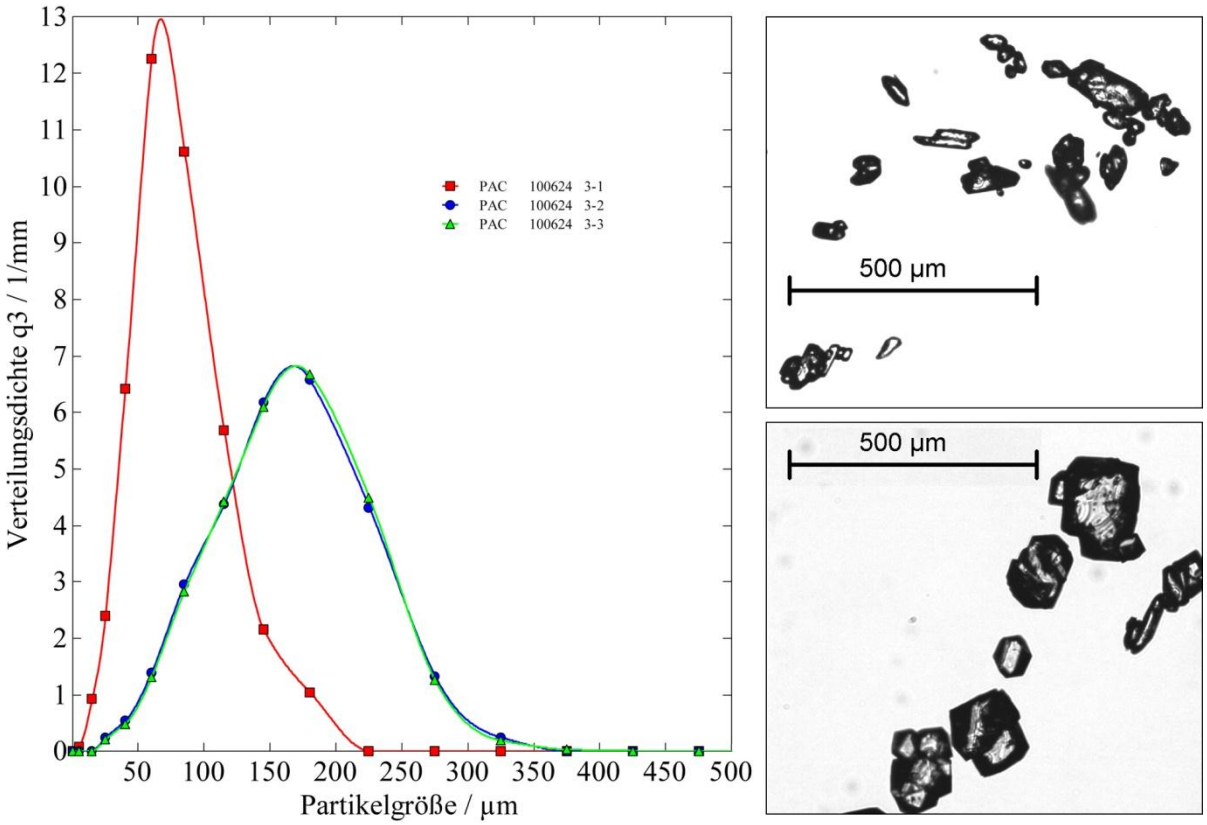

Figure 6-9: PAC, retention time 164 s

Table 6-6 shows data for the experiments at a retention time of 124 s. Due to smaller seed particles, the crystal growth in experiment **100625-2** is smaller than in experiment **100625-4**. The shift in seed particle size may result from classification in the supply vessel.

Table 6-6: PAC, retention time 124 s

Process parameters	pump settings	PI	17,8			PII	5	total flow	22,8	ml/min
	retention time								124	s
	waterbaths	T1	43	T2	39	T3	34	T4	28	T5	22	°C
ENr.	**100625-2**									
samples				1_{Seeds}		$2_{Product\ 1}$		$3_{Product\ 2}$		$4_{Seeds\ 2}$		
	t (sampling)			2		1		1		2	min
	mass			1,573		2,495		2,4466		1,874	g/min
	VMD			81,79		154,92		150,57		76,84	µm
calculation	m seed									0,8618	g/min
	m prod									2,4708	g/min
	VMD seed									79,315	µm
	VMD prod									152,745	µm
results	mass gain									287	%
	crystal growth									73,43	µm
ENr.	**100625-4**									
samples				1_{Seeds}		$2_{Product\ 1}$		$3_{Product\ 2}$		$4_{Seeds\ 2}$		
	t (sampling)			2		1		1		2	min
	mass			1,5014		2,0853		2,0698		1,5101	g/min
	VMD			111,6		221,32		218,86		119,14	µm
calculation	m seed									0,7529	g/min
	m prod									2,0776	g/min
	VMD seed									115,37	µm
	VMD prod									220,09	µm
results	mass gain									276	%
	crystal growth									104,72	µm

Figure 6-10 shows again a shift in particle size from seed to product crystals. The well-defined structure of product crystals proves that agglomeration and crystal-intergrowthplay only a subordinate role in the crystal growth.

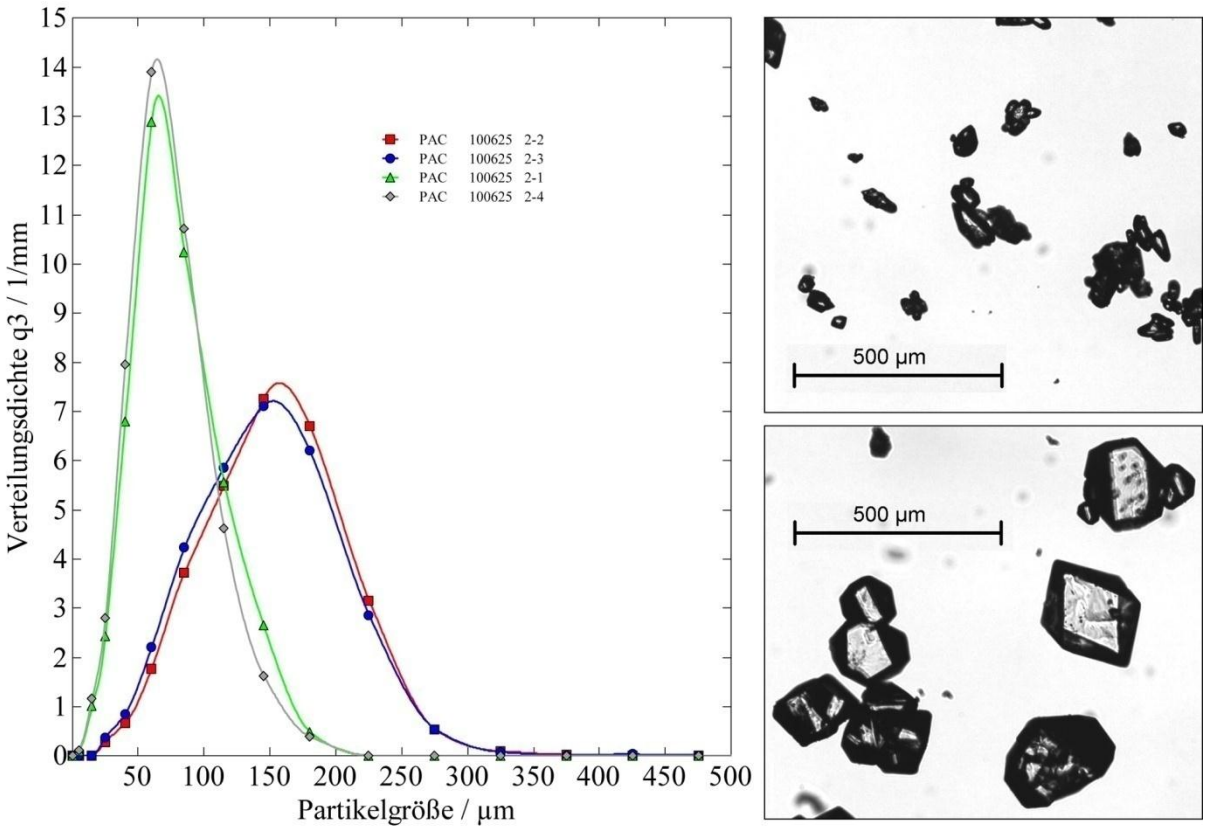

Figure 6-10: PAC, retention time 12 4s

Experiments with a retention time of 112 s led to crystal growth and mass gain as well. The results of these experiments are listed in **Table 6-7**.

Table 6-7: PAC, retention time 112 s

Process parameters	pump settings	PI	19,7		PII	5,5		total flow	25,2	ml/min
	retention time								112	s
	waterbaths	T1	43	T2 39	T3	34	T4 28	T5	22	°C

ENr.	**100628-1**					
samples		1_{Seeds}	$2_{Product\ 1}$	$3_{Product\ 2}$	$4_{Seeds\ 2}$	
	t (sampling)	2	1	1	2	min
	mass	1,7233	2,3376	2,3181	1,7178	g/min
	VMD	114,09	224,15	223,8	120,96	µm
calculation	m seed				0,8603	g/min
	m prod				2,3279	g/min
	VMD seed				117,525	µm
	VMD prod				223,975	µm
results	mass gain				271	%
	crystal growth				106,45	µm
ENr.	**100628-3**					
samples		1_{Seeds}	$2_{Product\ 1}$	$3_{Product\ 2}$	$4_{Seeds\ 2}$	
	t (sampling)	2	1	1	2	min
	mass	1,775	2,3577	2,3577	1,7183	g/min
	VMD	111,58	222,44	223,58	114,1	µm
calculation	m seed				0,8733	g/min
	m prod				2,3577	g/min
	VMD seed				112,84	µm
	VMD prod				223,01	µm
results	mass gain				270	%
	crystal growth				110,17	µm

Figure 6-11 shows the $q_3(x)$-distribution as well as seed and product particles for a retention time of 112 s.

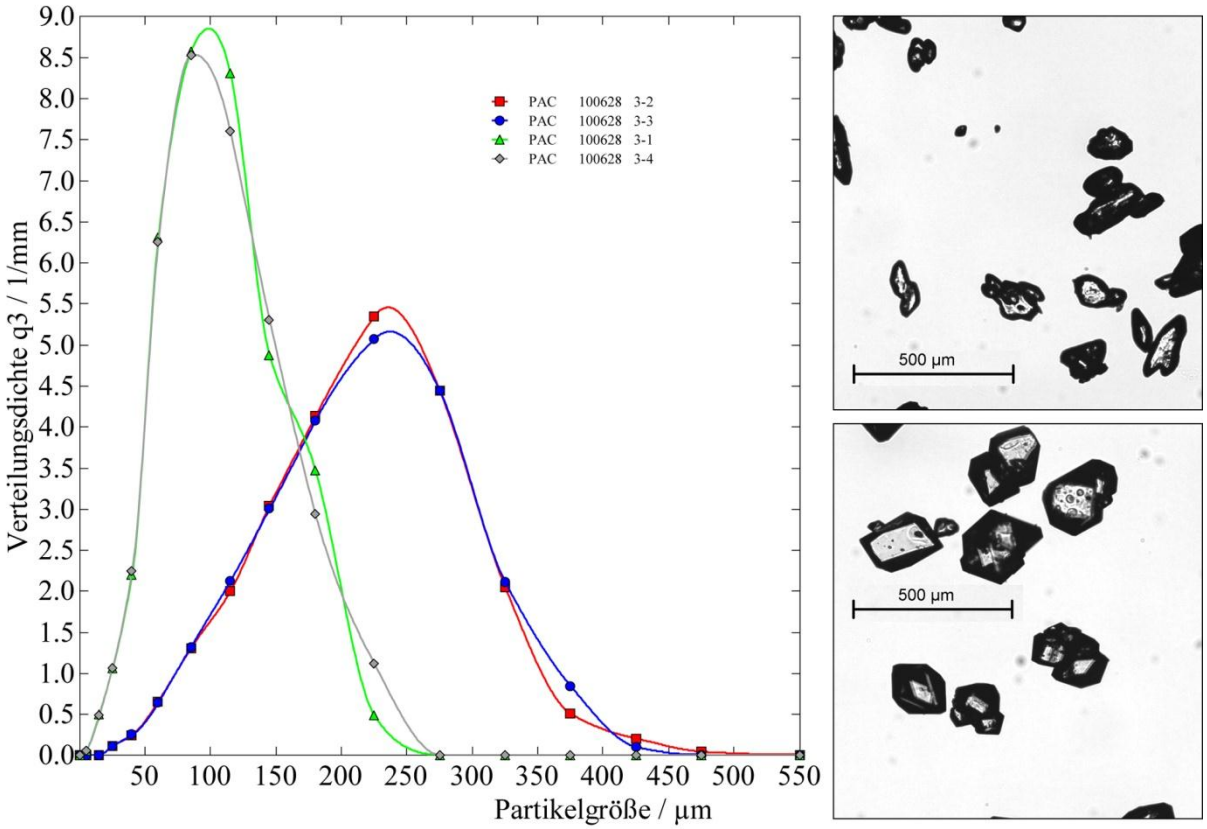

Figure 6-11: PAC, retention time 112s

6.2.2. COMPILATION OF RESULTS

The relationship between crystal growth and retention time is a well-grounded fact, but could not be obtained in the experiments. The reasons are mostly based on the different sizes of seed crystals. The experiments with lower retention times had been run with larger seed particles. This influence apparently overlays the dependence on the retention time. To underline the effect of the retention time, it needs to be varied in a larger range within the limits of laminar

flow. This could be easily implemented in further studies, because all experiments run accurately without blockage and are easy to handle.

Nevertheless, the influence of seed size is demonstrated in **Figure 6-12**.

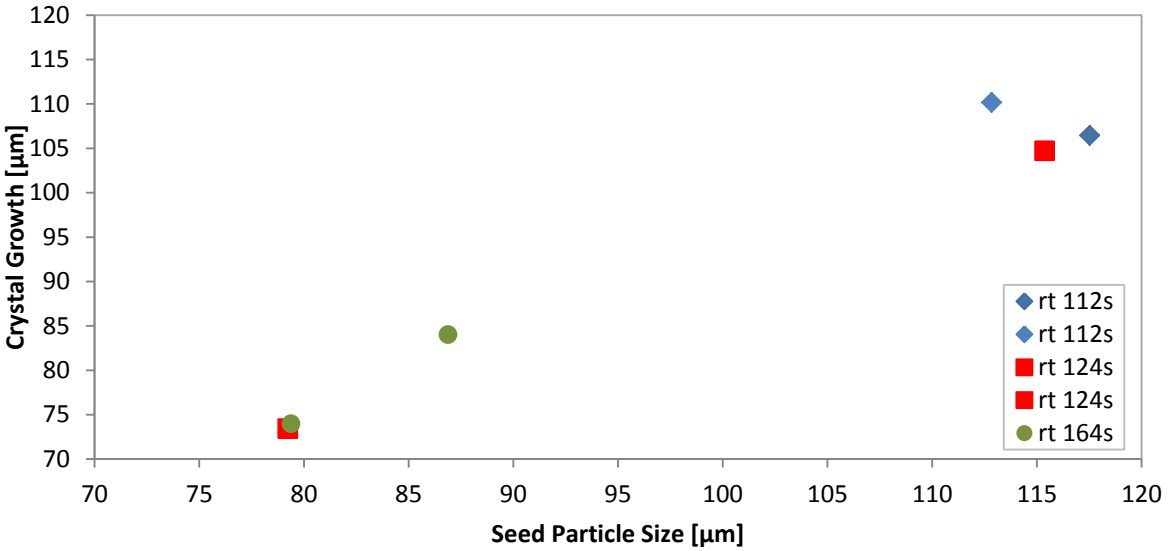

Figure 6-12: PAC, crystal growth for different seed particle sizes

The crystal growth in influenced by the seed size.

Even though the relationship between crystal growth and retention time could not be verified, the increase in mass gain is another evidence for the influence of the retention time. The experiments pointed out a slight, but detectable shift to higher mass gains with increasing retention times.

Figure 6-13 shows the mass gain for various retention times. The sizes of the diamonds demonstrate the different seed sizes and smaller seeds are marked by lighter colors.

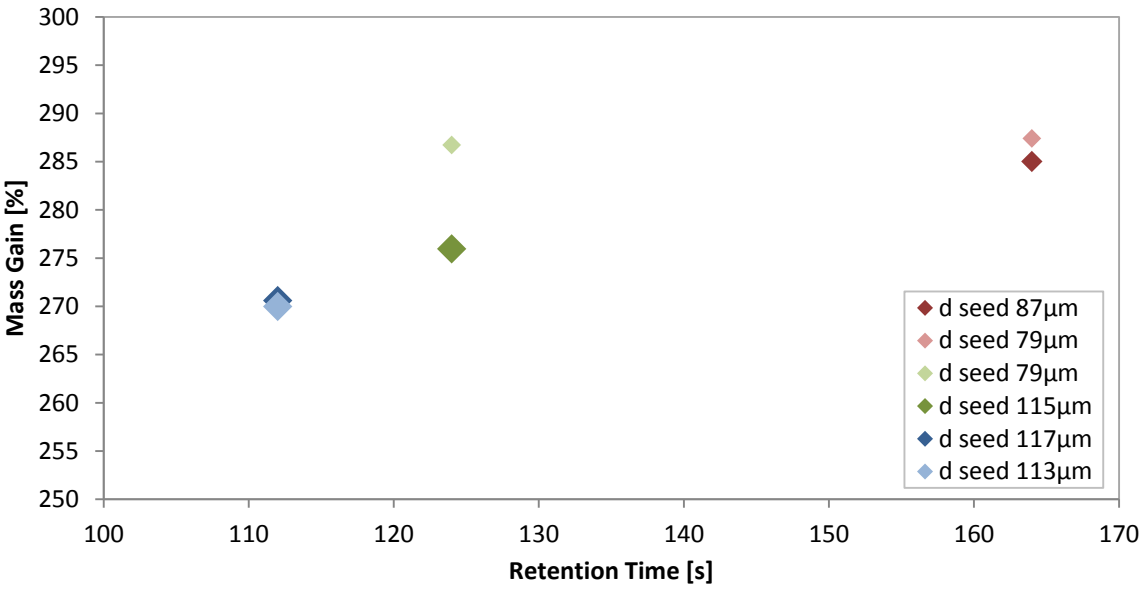

Figure 6-13: PAC, mass gain for various retention times

The shift of mass gain with increasing retention times can be demonstrated.

7. COMPARISON OF SIMULATED AND EXPERIMENTAL DATA

In this chapter, the limits of the simulation and possible sources of errors during the experiments are discussed.

Basically, the simulation was very helpful to get an overview about developing the cooling steps close to an optimized temperature profile. Furthermore, a prediction of crystal growth and mass gain could be made. The simulation disregards nucleation, agglomeration and crystal intergrowth, although these factors can strongly affect the process in reality. Moreover, the simulation is only valid for a batch of particles with exactly the same size and does not deal with particle size distributions.

On the other hand, the procedure of the experiments is associated with risks of errors, especially during the sampling process and crucial sample splitting for the analysis.

7.1. ASA

Figure 7-1 shows the comparison of simulated and experimental data for the crystal growth of ASA. The experimental results are marked by filled diamonds and dots, the simulated results by empty symbols, respectively.

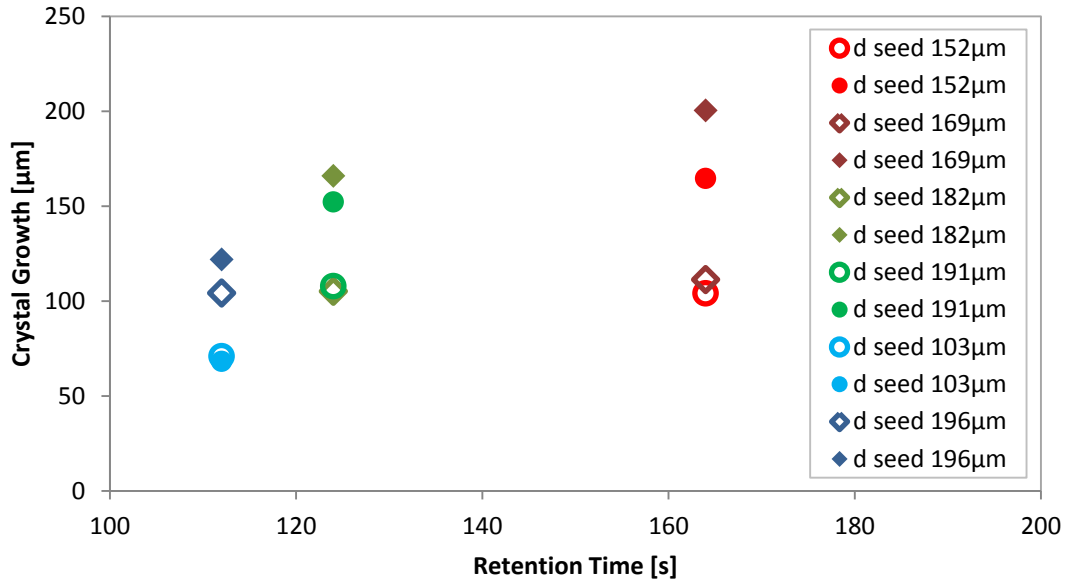

Figure 7-1: crystal growth of ASA, comparison of simulated (empty symbols) and experimental (filled symbols) data

Although the simulation predicts less crystal growth, the deviation to experimental data is almost constant for various retention times.

Generally the simulation does not predict as good results as obtained the corresponding experiments. This is caused by the presence of agglomeration in the experiments. Nevertheless the difference between simulated and experimental data is almost constant in the investigated range.

The increasing deviation of crystal growth with higher retention time may be caused by the simplifying assumption of no particle size distribution in the simulation. This leads to a negation of the effect that small particles are dissolved in favor of the growth of larger crystals. Hence this leads to an increased crystal growth, especially for higher retention times.

In previous experiments in the working group [1] the deviations are even less and agree well with the experimental data. In these experiments we forbear from excessive cooling.

Although the simulated data of the crystal growth do not confirm with the experiments, more similar results for the mass gain could be expected, as that the mass gain is not so much influenced by agglomeration. However, the comparison shown in **Figure 7-2** indicates a high deviation in mass gain due to secondary nucleation in the experiments. The more seeds are available from secondary nucleation, the larger the mass gain increases with longer retention times.

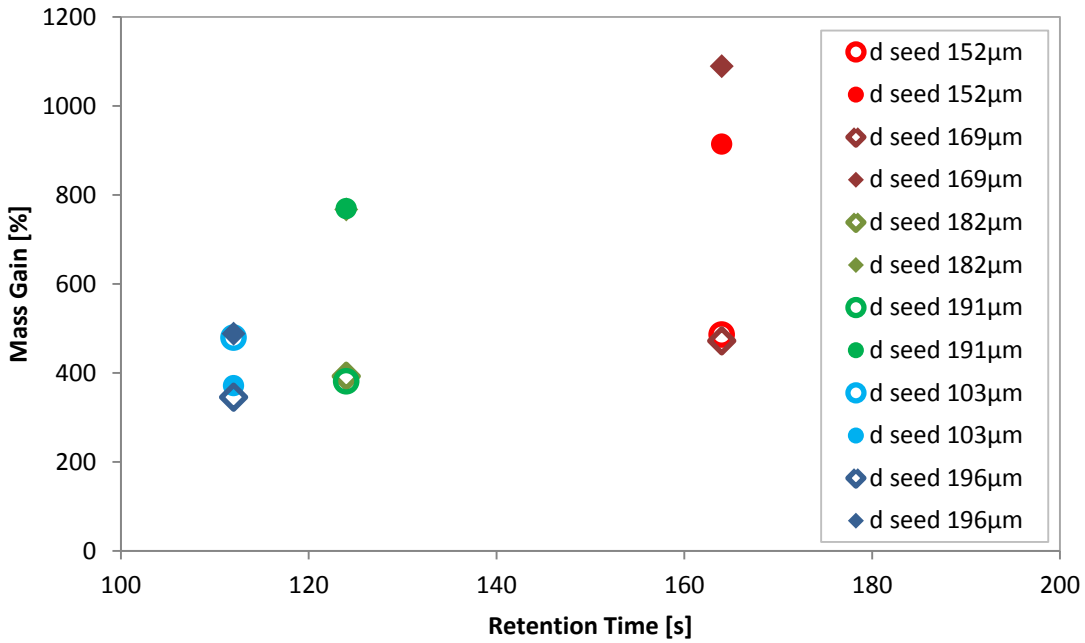

Figure 7-2: mass gain of ASA, comparison of simulated (empty symbols) and experimental (filled symbols) data

Due to nucleation, the deviation in mass gain is notable for experimental results.

7.2. PAC

Although we expected a proportional relationship between crystal growth and retention time, the influence of the seed particle size is huge. This fact is both proved by experimental and simulated data for PAC, as shown in **Figure 7-3**.

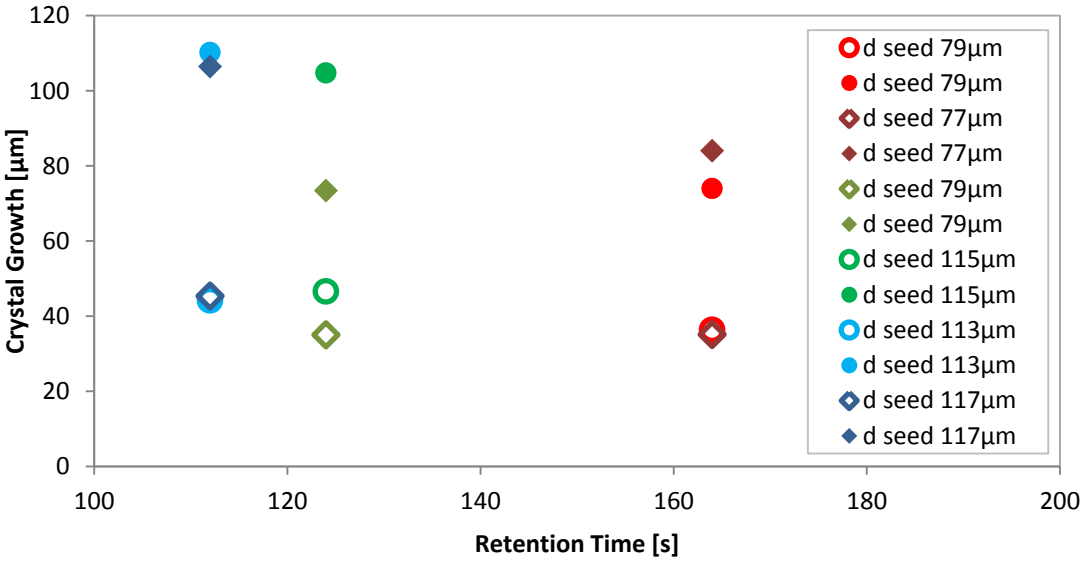

Figure 7-3: crystal growth of PAC, comparison of simulated (empty symbols) and experimental (filled symbols) data

The effect of the seed size has a stronger influence on the crystal growth than the retention time.

The comparison of experimental and simulated data of the mass gain of PAC (**Figure 7-4**) shows good agreement. The ordinate is finely subdivided to point out the deviations. These deviations probably range between statistical limits. Nevertheless, the simulation shows higher values for higher retention times than the corresponding experiments. This can be caused by sampling errors.

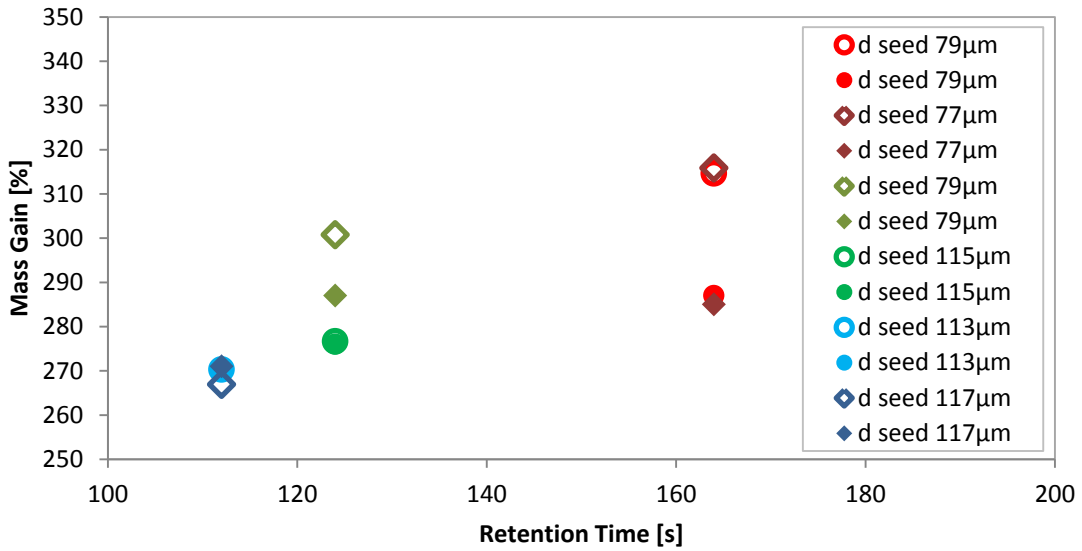

Figure 7-4: mass gain of PAC, comparison of simulated (empty symbols) and experimental (filled symbols) data

Simulated and experimental data show good agreement. Increasing deviations with higher retention times are caused by the sampling procedure during the experiments.

8. CONCLUSION AND OUTLOOK

In this work a continuously seeded, continuously operated tubular crystallizer system (CSCOTC) was used for the crystallization of active pharmaceutical ingredients (APIs). The crystallizer consists of a silicone tube with a length of 15 m and an inner diameter of 2 mm, fed by a mixture of a seed suspension stream and a feed stream. The feed stream was a slightly undersaturated solution of the model substance, kept at an elevated temperature to guarantee the absence of solid particles. The seed suspension stream contained a defined mass of solid particles which grew while passing the reactor. The supersaturation level along the reactor, which was created by cooling, was responsible for the growth of the crystals. To ensure a constantly rising supersaturation, a cooling trajectory consisting of five, independently controlled waterbaths was developed. Therefore, a simulation in MatLab® was used. Furthermore, the influence of the retention time as well as the initial seed particle size was simulated.

Acetylsalicylic acid (ASA) and paracetamol as model substances were crystallized from an ethanolic solution. The investigation of paracetamol necessitated the adaption of the process parameters to its solubility behavior.

This work comprises the development of an optimized cooling trajectory, the adaption of the process to a new model substance, the study of the influence of the retention time and the simulation of all parameters for both substances in MatLab®.

Simulation

By using the simulation, an optimized temperature profile of the cooling trajectory was developed. The basic condition for the optimization was an increasing supersaturation level along the tubing, as the supersaturation is the driving force for crystallization. Hence the supersaturation level can be raised in the presence of larger crystals without running the risk of nucleation and therefore blocking of the reactor. This leads to the formation of larger crystals. The supersaturation strongly depends on the temperature, so the supersaturation level

can be increased by cooling the solution. In a segmented cooling trajectory of five waterbaths, the cooling steps have to become steeper along the tubing.

The simulation of the crystallization of paracetamol had to be adapted to the different solubility behaviour and then used to acquire the temperatures of the cooling baths.

After setting all parameters, the influence of the retention time and the seed particle size on the crystal growth could be simulated.

The retention time was varied between 112 s, 124 s and 164 s while the seed particle size was kept constant. As expected, the product crystals underwent a stronger growth at higher retention times. The crystal growth followed a logarithmic function; however the curve can be sufficiently fitted by a linear expression in the investigated range.

Nevertheless the influence of the initial seed size cannot be neglected. According to the theory at constant retention times smaller crystals experience a minor growth than larger crystals, due to their higher volume-to-mass ratio. The simulation figured out that even small deviations in the seed size significantly superpose the dependence of the retention time.

According to that, further detailed research includes the development of a simulation which permits both the particle size distribution of seeds and the population balance in the reactor.

Investigation of ASA

The new temperature profile could be successfully implemented in the laboratory. Though during the test runs crystallization itself was difficult to handle, because of agglomeration and crystal intergrowth, single particle sizes up to 500 µm (25% of the inner diameter of the reactor) could be achieved. This is why the risk of blocking considerably increased, especially the last part of the reactor in the coldest waterbath. To solve this problem, the temperature of the last waterbath was raised by 2 °C compared to the simulation. So blocking could be avoided successfully.

The results of the experiments clearly verify the influence of the retention time. With higher retention times, the crystal growth increased. However, due to the batch-wise preparation of seeds, the initial seed sizes could not be kept constant; therefore the influence of the seed size on the crystal growth is not negligible. The comparison of the experimental results clearly showed an increasing crystal growth for higher retention times and larger seed crystals.

In the presented work, the crystal growth of ASA was extensively tested. In the future the seed precipitation is worth being investigated in due detail. Aditionally, an in-situ-production

of seeds in the existing crystallizer is feasible, as pointed out in two experiments. The required process parameters for this procedure could be ascertained in further studies. This can lead to smaller deviations in the seed sizes and to an increased reproducibility.

Investigation of Paracetamol

The adaption of the reactor to the new model substance paracetamol proceeded smoothly without any problems. All obtained parameters from the simulation could be kept. The temperature profile could be followed without blocking the reactor, so all experiments were run successfully.

Only the preparation was challenging: the seeds were very small and showed considerable deviations in size. As already known from the simulation, the crystal growth is only marginally dependent on the retention time for small seeds sizes. Even for paracetamol, deviations in seed sizes strongly influence the crystal growth, based on the smaller dependence of the solubility on the temperature. The crystal growth therefore cannot be conclusively attributed to the influence of the retention time. In return, the influence of the seed size was confirmed again.

Further experiments with paracetamol allow a number of more detailed key studies. The reproduction of a narrow seed size distribution seems to be a promising field to investigate. Furthermore some parameters of the process control are still open for optimization; particularly the temperatures of the feed stream could be raised to permit a steeper temperature profile, which allows a better utilization of the supersaturation.

REFERENCE LIST

(1) R. J. P. Eder, E. K. Schmitt, J. Grill, S. Radl, H. Gruber-Woelfler et al. Seed Loading Effects on the Mean Crystal Size of Acetylsalicylic Acid in a Continuous-Flow Crystallization Device. Crystal Research and Technology. 2011; 46: 227-237

(2) Eder RJP, Radl S, Schmitt E, Innerhofer S, Maier M, Gruber-Woelfler H et al. Continuously Seeded, Continuously Operated Tubular Crystallizer for the Production of Active Pharmaceutical Ingredients. Crystal Growth & Design. 2010; 10:2247-2257.

(3) Alvarez Aj, Myerson AS. Continuous Block Flow Crystallization of Pharmaceutical Compounds. Crystal Growth & Design. 2010; 10:2219-2228.

(4) Lawton S, Steele G, Shering P Continuous Crystallization of Pharmaceuticals Using a Continuous Oscillatory Baffled Crystallizer. Organic Process Research & Development 2009, 13: 1357–1363

(5) Maia GD, Giulietti M. Solubility of acetylsalicylic acid in ethanol, acetone, propylene glycol, and 2-propanol. Journal of Chemical and Engineering Data. 2008; 53:256-258.

(6) Variankaval N, Cote AS, Doherty MF. From form to function: Crystallization of active pharmaceutical ingredients. Aiche Journal. 2008; 54:1682-1688.

(7) Dombrowski RD, Litster JD, Wagner NJ, He Y. Crystallization of alpha-lactose monohydrate in a drop-based microfluidic crystallizer. Chemical Engineering Science. 2007; 62:4802-4810.

(8) Su YF, Kim H, Kovenklioglu S, Lee WY. Continuous nanoparticle production by microfluldic-based emulsion, mixing and crystallization. Journal of Solid State Chemistry. 2007; 180:2625-2629.

(9) Cui Y. A material science perspective of pharmaceutical solids. International Journal of Pharmaceutics. 2007; 339:3-18.

(10) Oullion M, Puel F, Fevotte G, Righini S, Carvin P. Industrial batch crystallization of a plate-like organic product. In situ monitoring and 2D-CSD modelling: Part 1: Experimental study. Chemical Engineering Science. 2007; 62:820-832.

(11) Méndez del Rio JR, Rousseau RW. Batch and tubular-batch crystallization of paracetamol: Crystal size distribution and polymorph formation. Crystal Growth & Design. 2006; 6:1407-1414.

(12) Gerdts CJ, Tereshko V, Yadav MK, Dementieva I, Collart F, Joachimiak A et al. Time-controlled microfluidic seeding in nL-volume droplets to separate nucleation and growth stages of protein crystallization. Angewandte Chemie-International Edition. 2006; 45:8156-8160.

(13) Hofmann Guenter. Kristallisation in der Industriellen Praxis. Weinheim: Wiley-VCH, 2004.

(14) Mazzotti M, Worlitschek J. Model-Based Optimization of Particle Size Distribution in Batch-Cooling Crystallizer of Paracetamol. Crystal Growth & Design. 2004; 6:891-903.

(15) Brenek SJ, AM Ende DJ. Crystallization method and apparatus using an impinging plate assembly. US Patent. 2004; 0040098839.

(16) Schiewe J, Zierenberg B. Process and apparatus for producing inhalable medicaments. US Patent. 2003; 2003/0015194A1.

(17) Myerson AS. Molecular crystals of controlled size. US Patent. 2003; 0030170999.

(18) Myerson AS. Handbook of Industrial Crystallization. 2nd ed. Boston Oxford Johannesburg Melbourne New Delhi Singapore: Butterworth-Heinemann, 2002.

(19) Rasmuson A, Gracin S. Solubility of Phenylacetic Acid, p-Hydroxyphenylacetic Acid, p-Aminophenylacetic Acid, p-Hydroxybenzoic Acid, and Ibuprofen in Pure Solvents. Journal of Chemical Engineering Data. 2002; 47: 1379-1383

(20) Gros H, Kilpiö T, Nurmi J Continuous cooling crystallization from solution. Powder Technology. 2001; 121: 106-115

(21) Kirklin DR. Enthalpy of combustion of acetylsalicylic acid. Journal of Chemical Thermodynamics. 2000; 32:701-709.

(22) Beckmann W. Seeding the desired polymorph: Background, possibilities, limitations, and case studies. Organic Process Research & Development. 2000; 4:372-383.

(23) Granberg R., Rasmuson A Solubility of Paracetamol in Pure Solvents. Journal of Chemical Engineering Data. 1999; 44: 1391-1395

(24) Yu L, Reutzel SM, Stephenson GA. Physical characterization of polymorphic drugs: an integrated characterization strategy. Pharmaceutical Science & Technology Today. 1998; 1:118-127.

(25) Mullin JW. Crystallization. 3rd ed. Oxford Boston Johannesburg Melbourne New Delhi Singapore: Butterworth-Heinemann, 1992.

(26) Midler MJr, Liu PD, Paul EL, Futran M, Whittington EF. A crystallization method to improve crystal structure and size. EP. 1991; 0461930A1.